CANCER

The metabolic adaptation evoked by arginine enhances the effect of radiation in brain metastases

Rossella Marullo[1]†, Monica Castro[2]†, Shira Yomtoubian[3,4], M. Nieves Calvo-Vidal[1], Maria Victoria Revuelta[1], Jan Krumsiek[5], Andrew Cho[6], Pablo Cresta Morgado[2], ShaoNing Yang[1], Vanina Medina[7,8], Berta M. Roth[9], Marcelo Bonomi[10], Kayvan R. Keshari[6,11,12], Vivek Mittal[3,4], Alfredo Navigante[2]‡, Leandro Cerchietti[1]*‡

Selected patients with brain metastases (BM) are candidates for radiotherapy. A lactatogenic metabolism, common in BM, has been associated with radioresistance. We demonstrated that BM express nitric oxide (NO) synthase 2 and that administration of its substrate L-arginine decreases tumor lactate in BM patients. In a placebo-controlled trial, we showed that administration of L-arginine before each fraction enhanced the effect of radiation, improving the control of BM. Studies in preclinical models demonstrated that L-arginine radiosensitization is a NO-mediated mechanism secondary to the metabolic adaptation induced in cancer cells. We showed that the decrease in tumor lactate was a consequence of reduced glycolysis that also impacted ATP and NAD$^+$ levels. These effects were associated with NO-dependent inhibition of GAPDH and hyperactivation of PARP upon nitrosative DNA damage. These metabolic changes ultimately impaired the repair of DNA damage induced by radiation in cancer cells while greatly sparing tumor-infiltrating lymphocytes.

INTRODUCTION

Brain metastases (BM) occur in 10 to 20% of adult patients with solid tumors—melanoma, non–small cell lung cancer (NSCLC), and triple-negative breast cancer (TNBC) in particular—accounting for up to three quarters of metastatic brain lesions (1, 2). Development of BM is associated with short overall survival (OS), and their occurrence is a major cause of morbidity due to progressive neurologic deficits that result in a reduced quality of life (2, 3). For selected patients, this outcome can be improved by achieving greater local control (1, 2). Radiation is the most common treatment received by patients with BM, either as part of their primary treatment or with adjuvant or palliative intent (1). Agents that increase the sensitivity of cancer cells to radiation may further improve the control of the disease; however, the blood-brain barrier represents a substantial pharmacological challenge for most compounds (1). Nitric oxide (NO) is a gaseous, stable free radical with signaling activities that regulate physiological and pathological processes. Relatively high concentrations of NO have been shown to induce chemo- and radiosensitization in preclinical models and patients with solid tumors (4–9), and this effect has also been observed in hypoxic tumors (9–11). Although the mechanism of the NO-induced radiosensitization is not fully elucidated, it is currently accepted that NO can radiosensitize tumors by increasing the tumor blood flow (TBF) and by decreasing tumor oxygen consumption, an effect particularly relevant in hypoxic conditions (8, 12–14).

An increase in NO content of tumors can be achieved by direct use of NO donors or by stimulation of the endogenous pathway producing this radical (15). Previous experiences with animal models and treatment of noncancer patients have shown that spontaneous and bioreductive donors provoke potentially severe side effects, mostly as a consequence of systemic hypotension (15). Moreover, systemic vasodilatation can decrease TBF, making tumors more hypoxic and acidic (16, 17) and potentially overruling the radiation sensitizer property of NO. An alternative therapeutic strategy to increase NO production is to administer L-arginine, the endogenous substrate of NO synthase (NOS) (15). Of the three isoforms of NOS, NOS2 is transcriptionally up-regulated in inflammatory conditions and hypoxia; thus, it is more likely to be expressed in tumor tissues. In estrogen receptor–negative breast cancer patients, NOS2 expression in primary tumors is associated with disease progression (18), and in a murine xenograft model of TNBC, NOS2 activity is required for developing BM (19). Although NOS-derived NO represents a survival advantage for cancer cells (20), tumors must constantly fine-tune the production of NO to avoid the cytotoxicity derived from overproduction of NO and its metabolites (20–22).

Administration of L-arginine has been shown to increase NO production and improve clinical parameters in patients with diseases associated with endothelial dysfunction (23–25). Accordingly, several studies in patients with genetic mitochondrial syndromes such as MELAS (myopathy, encephalopathy, lactic acidosis, and stroke-like episodes) have shown that administration of L-arginine results in increased NO production, improved microcirculation in the cerebral blood flow, and decreased frequency and severity of

[1]Hematology and Oncology Division, Weill Cornell Medicine, Cornell University, New York, NY, USA. [2]Translational Research Unit, Angel Roffo Cancer Institute, University of Buenos Aires, Buenos Aires, Argentina. [3]Department of Cardiothoracic Surgery, Weill Cornell Medicine, Cornell University, New York, NY, USA. [4]Department of Cell and Developmental Biology, Weill Cornell Medicine, Cornell University, New York, NY, USA. [5]Department of Physiology and Biophysics, Institute for Computational Biomedicine, Weill Cornell Medicine, New York, NY, USA. [6]Department of Biochemistry and Structural Biology, Weill Cornell Graduate School, New York, NY, USA. [7]Laboratory of Tumor Biology and Inflammation, Institute for Biomedical Research, School of Medical Sciences, Pontifical Catholic University of Argentina and National Scientific and Technical Research Council, Buenos Aires, Argentina. [8]Laboratory of Radioisotopes, School of Pharmacy and Biochemistry, University of Buenos Aires, Buenos Aires, Argentina. [9]Radiation and Imaging Department, Angel Roffo Cancer Institute, University of Buenos Aires, Buenos Aires, Argentina. [10]Hematology and Oncology Division, The Ohio State University, Columbus, OH, USA. [11]Department of Radiology, Memorial Sloan Kettering Cancer Center, New York, NY, USA. [12]Molecular Pharmacology Program, Memorial Sloan Kettering Cancer Center, New York, NY, USA.
*Corresponding author. Email: lec2010@med.cornell.edu
†These authors contributed equally to this work.
‡These authors contributed equally to this work.

stroke-like episodes (*26–28*). Moreover, oral L-arginine is recommended to reduce the risk of recurrent stroke-like episodes in patients with MELAS (*28*). Together, these studies indicated that L-arginine administration results in NO production at therapeutic levels while minimizing unwanted hemodynamic effects associated with pharmacological NO donors.

Here, we show that administration of oral L-arginine results in radiosensitization and improved local control in patients with BM from solid tumors for whom the standard of care involves radiation therapy. In preclinical cancer models, we demonstrated that this effect is a consequence of an increased vulnerability to DNA damage in NOS2-expressing cancer cells that results from NO-induced metabolic suppression.

RESULTS

L-Arginine decreases tumoral lactate content in patients with BM

To exploit the arginine-NO axis to radiosensitize BM, we first assessed the expression of NOS isoforms associated with tumors. The expression of inducible NOS2 has been reported in cancer cells and tumor microenvironment (TME) cells in lung and breast cancers (*18*, *20*, *29*, *30*), whereas NOS3 expression has been found limited to tumor-associated endothelial cells (*31*). In a cohort of 42 patients with BM derived from NSCLC (40%), TNBC (19%), and other solid tumors (41%), we detected NOS3 expression in tumor-associated blood vessels (see fig. S1A for a representative image) and NOS2 expression in both cancer and TME cells (Fig. 1A). Overall, 88% of
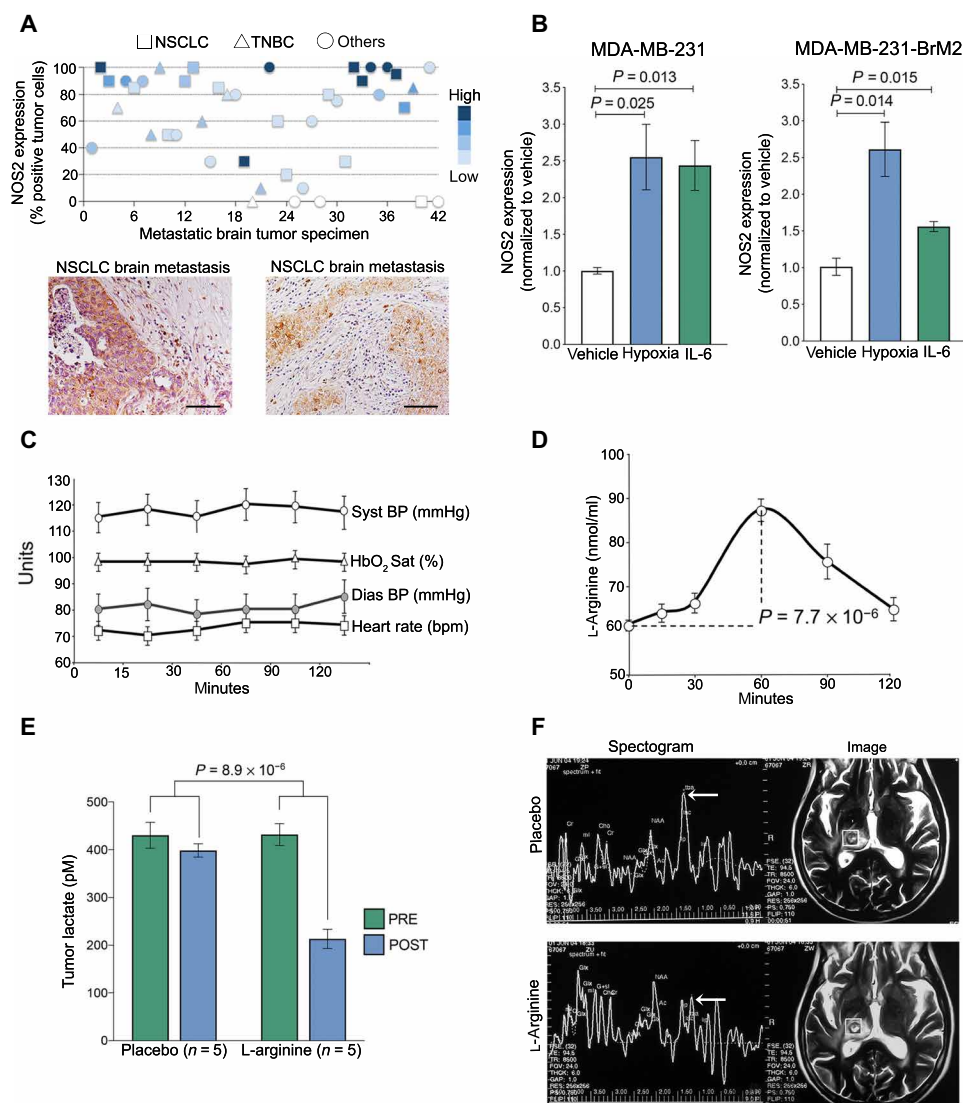
Fig. 1. L-Arginine decreases tumor lactate concentration in BM. (**A**) Expression of NOS2 in 42 BM specimens. The *Y* axis indicates the percent of positive cells, the color scale represents intensity of expression, and the shape represents different origins of the primary tumor. Representative immunohistochemistry images of two patients with BM from NSCLC. Scale bars, 100 μm. (**B**) NOS2 expression in MDA-MB-231 and MDA-MB-231-BrM2 cells treated with interleukin-6 (IL-6) and hypoxia (1% O_2). (**C**) Hemodynamic parameters obtained from five patients treated with a single oral dose of 10 g of L-arginine. (**D**) Plasma concentration of L-arginine obtained from patients in (C). (**E**) Quantification of tumor lactate in BM before (PRE) and after (POST) administration of placebo (*n* = 5) and L-arginine (*n* = 5) taken 24 hours apart. (**F**) Representative magnetic resonance spectrograms and corresponding images from a patient with BM treated with placebo (top) and 24 hours later with L-arginine (bottom). The arrow indicates the lactate peak.

BM expressed NOS2 with 19% of them at high levels, with no association with the type of primary tumor (Fig. 1A). Because expression of NOS2 can be further induced by TME conditions common in BM such as hypoxia and inflammation (*32*), we determined whether these stimuli will further induce NOS2 expression. We used the TNBC cell line MDA-MB-231 and its BM-derived cell line MDA-MB-231-BrM2 (*33*) and exposed them to hypoxia [PO_2 (partial pressure of oxygen) = 1%, 3 hours] or interleukin-6 (IL-6) (40 nM, 3 hours). We found that both stimuli, prevalent in the TME, increased the expression of NOS2 in both cell lines (Fig. 1B).

We then investigated whether the vascular and metabolic effects of L-arginine administration described in other clinical settings were also evident in patients with BM. L-Arginine can be administered by oral or intravenous routes (*34*); however, we considered the oral route potentially more feasible in our intended clinical context. The oral bioavailability of L-arginine in healthy subjects is around 62% (*35*), and once in plasma, approximately 54% of the L-arginine is converted to NO, while 5 to 6% contributes to synthesis of urea (*36*). As a single dose in solution, L-arginine is tolerable between 5 and 10 g (*37*). To assess whether 10 g of L-arginine was tolerable to BM patients and sufficient to induce a significant increase in plasma levels, we determined its pharmacokinetic profile in five patients with BM. Patients were premedicated for nausea and vomiting and received a single 10-g oral dose of L-arginine in water solution. L-Arginine was well tolerated, with patients reporting an unpleasant aftertaste. There were no discernible effects on arterial tension or heart rate during a 120-min observation (Fig. 1C). This dose was enough to cause an increase in plasma L-arginine to 87.2 ± 1.7 nmol/ml at 1 hour from 61.1 ± 0.8 nmol/ml at baseline, representing a mean 42% increase ($P < 0.001$) (Fig. 1D). The tumor vascular effects of 10 g of oral L-arginine were evaluated in five patients with BM. We determined the tumor blood volume (TBV) and TBF by perfusion-weighted magnetic resonance imaging (MRI) before and 1 hour after L-arginine administration. We found that although L-arginine did not significantly change the TBF (pre: 0.82 ± 0.58 versus post: 0.70 ± 0.22, $P =$ not significant), the TBV significantly decreased after the treatment [pre: 1.92 ± 1.10 versus post: 1.00 ± 0.37, $P = 0.03$, analysis of variance (ANOVA); fig. S1B]. Noteworthy, the dispersion of the TBV measurements also decreased after L-arginine treatment (a representative case is shown in fig. S1B), which could be suggestive of a transient homogenization in BM microvascular hemodynamics.

To determine tumor metabolic effects of L-arginine, we measured the tumor lactate concentration, a biomarker and driver of radioresistance by magnetic resonance spectroscopy (MRS). To allow an adequate washout of the contrast agent, pre– and post–L-arginine studies were performed 24 hours apart with the L-arginine (or placebo) administered on the second day 1 hour before the MRS scan. To control for unspecific changes during this 24-hour period, the patients were randomized to placebo ($n = 5$) or L-arginine ($n = 5$). We found that the tumor lactate concentration was consistently and significantly reduced after L-arginine administration compared to placebo (Fig. 1, E and F). Pre– and post–L-arginine tumor lactate concentrations were 430.4 ± 27 pM versus 398.6 ± 14 pM in placebo, and 431.8 ± 22.8 pM versus 213.2 ± 20.3 pM in L-arginine patients ($P < 0.0001$, *t* test; Fig. 1E). To assess a possible contribution of diminished glucose uptake to this effect, we conducted fludeoxyglucose (^{18}F) positron emission tomography (PET) in BM patients before and after administration of oral L-arginine ($n = 5$). ^{18}F-PET scans were performed at baseline on day 1 and 1 hour after the administration

of L-arginine on day 2. We found no significant differences in fludeoxyglucose uptake under these conditions (pre–L-arginine SUV^{max}: 10.9 ± 3 versus post–L-arginine SUV^{max}: 11.2 ± 5; a representative case is shown in fig. S1C), suggesting that the decrease in lactate levels is unlikely to be secondary to a decrease in the glucose uptake in BM but rather consequent to decreasing lactate production in tumor cells.

L-arginine induces radiosensitization in patients with BM

Considering these findings, we conducted a proof-of-concept randomized clinical trial to determine whether L-arginine increases the effect of radiation therapy in patients with unresectable BM from solid tumors. From 67 BM patients eligible for the study, 4 were excluded because they rejected the treatment, and the remaining 63 patients were randomized to oral L-arginine (10 g) ($n = 31$) or placebo ($n = 32$) 1 hour before each radiation fraction (Fig. 2A). Radiation treatment consisted of 32 Gy administered in 20 fractions of 1.6 Gy bidaily, followed by a 22.4-Gy boost with the same fractionation schedule. Overall, patients enrolled in the study had high-risk disease because the majority had uncontrolled primary tumor, multiple metastatic sites, and multiple BM (table S1). The median follow-up, defined as the median interval from the end of the treatment to the time of the analysis, was 5 months (range, 1 to 55 months). All patients completed the whole-brain radiotherapy and were fully assessable for toxicity and response.

L-arginine was well tolerated and did not increase short- or long-term (after 6 months) adverse events (table S2). There were no L-arginine–related grade 3 or 4 toxicities or deaths. The outcomes of the patients treated with L-arginine and placebo for the intent-to-treat analysis are shown in Table 1. The overall response rate was 22% (7 of 32) and 77.4% (24 of 31) for placebo and L-arginine arms, respectively ($P < 0.001$, Fisher's exact test; Fig. 2B and Table 1). The symptomatic response rate was 50% (16 of 32) and 93.5% (29 of 31) for placebo and L-arginine arms, respectively ($P = 0.002$, Fisher's exact test; Table 1). There were more complete neurological responses in patients receiving L-arginine (29% versus 9.4% in placebo; $P = 0.059$, Fisher's exact test; Table 1). This translated into increased number of patients free from neurological progression at 6 months in the L-arginine arm compared to the placebo arm (82% versus 20%; $P < 0.0001$, Cox-Mantel test; Fig. 2C). The median overall progression-free survival (PFS) was 2 months (range, 0 to 4 months) and 5 months (range, 4 to 6 months) for placebo and L-arginine arms, respectively ($P = 0.0007$, Cox-Mantel test; fig. S2). The differences in duration of neurological and overall PFS between the treatment groups indicate that most of the patients in the L-arginine group died as a consequence of the progression of the extracranial disease. There were exceptional responders among patients with no extracranial disease in the L-arginine arm (Fig. 2D). Overall, these results indicate that oral L-arginine is a feasible and possible effective strategy to induce radiosensitization in patients with BM.

L-Arginine causes suppression of tumor metabolism in preclinical TNBC models

To further characterize the metabolic changes induced by L-arginine, we conducted tumor metabolomic studies in the TNBC cell lines MDA-MB-231 and MDA-MB-468 implanted in mice. Once tumors reached palpable size, mice were randomized to receive either a mouse-equivalent dose of oral L-arginine or vehicle; after 1 hour, the tumors were extracted and processed for untargeted metabolomic analysis (Fig. 3A). Compared to vehicle, L-arginine significantly changed the
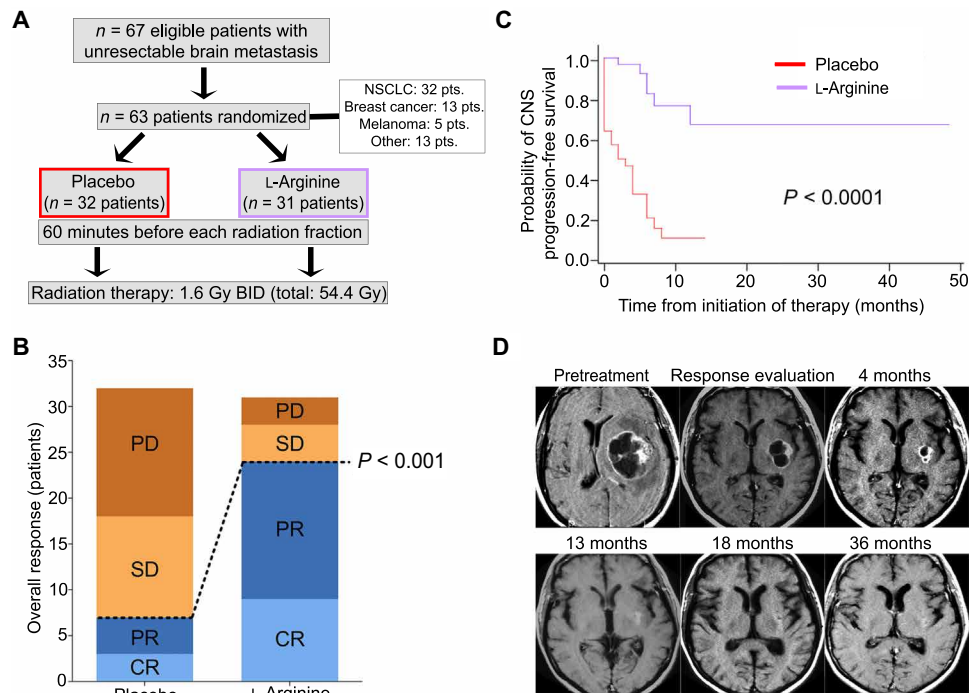
Fig. 2. L-Arginine improves the effect of radiation therapy in patients with BM. (**A**) Flowchart of clinical trial design with allocation results. (**B**) Overall responses as number of patients achieving a response category by allocation arm. The *P* value represents the comparison of complete (CR) plus partial responses (PR) among arms. PD, progressive disease; SD, stable disease. (**C**) Kaplan-Meier curves of the probability of central nervous system (CNS) progression-free survival in L-arginine and placebo arms. (**D**) Representative images from an NSCLC patient with BM enrolled in the L-arginine arm of the clinical trial.

Table 1. Clinical trial outcome. NA, Not assessed.

Variable	Placebo		L-Arginine		P
	No.	%	No.	%	
Total number of evaluable patients	32		31		
Radiological responses					
Complete	3	9.4	9	29	0.059 (C)
Partial	4	12.5	15	48.4	<0.001 (C + P)
Stable	11	34.4	4	13	
Progression	5	16	1	3.2	
NA	9	28.2	2	6.4	
Symptomatic responses					
Complete	10	31.2	25	80.6	
Partial	6	18.8	4	13	0.002 (C + P)
Stable	4	12.5	1	3.2	
Progression	12	37.5	1	3.2	
NA	0		0		
Overall responses					
Complete	3	9.4	9	29	0.059 (C)
Partial	4	12.5	15	48.4	<0.001 (C + P)
Stable	11	34.4	4	13	
Progression	14	43.7	3	9.6	
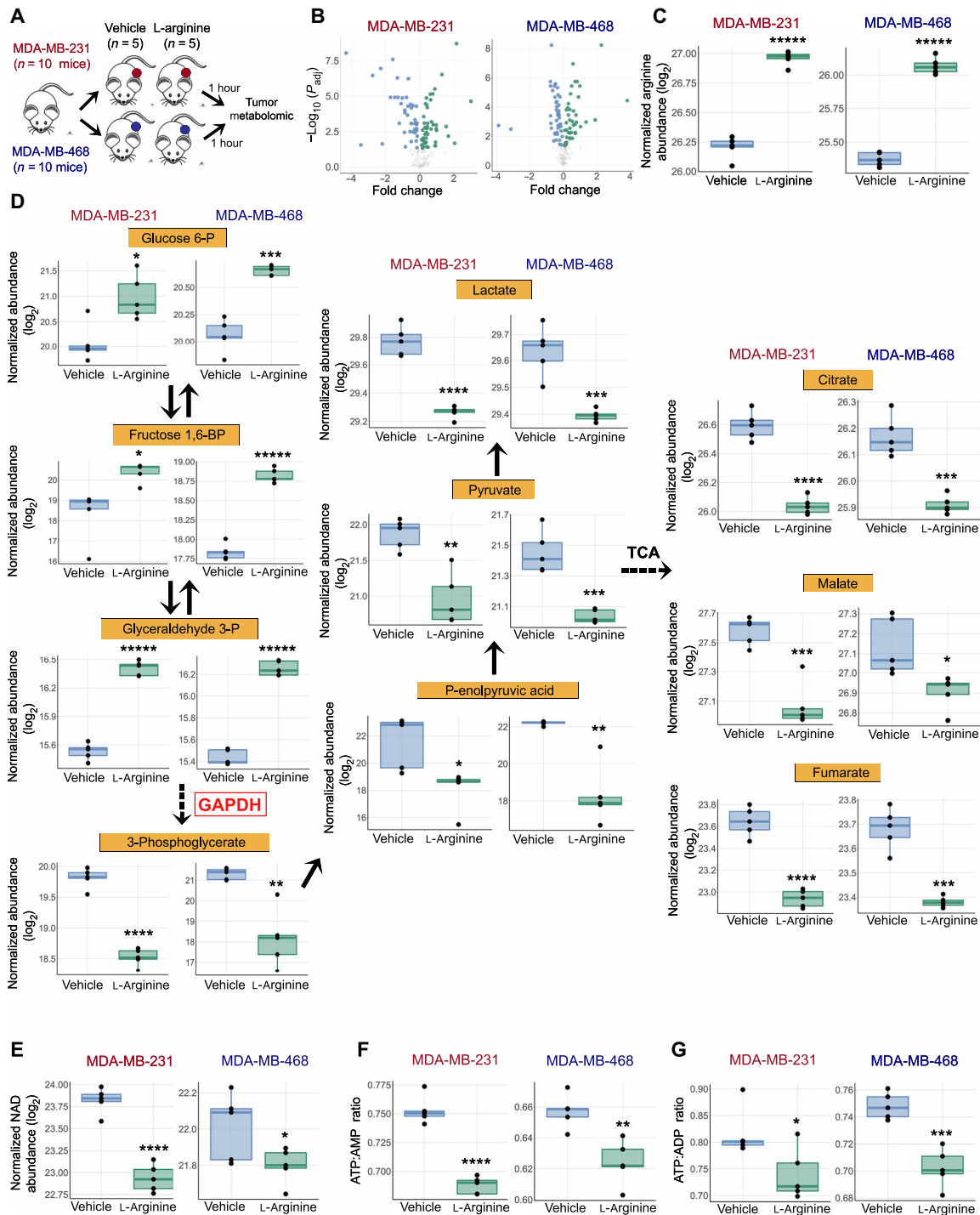
Fig. 3. Cellular metabolic changes induced by L-arginine administration in TNBC models. (**A**) Schematic representation of experiments using two TNBC xenograft models. (**B**) Volcano plots displaying metabolites significantly changed in vehicle- versus L-arginine–treated MDA-MB-231 and MDA-MB-468 xenografts. (**C**) Boxplot of L-arginine levels in vehicle- versus L-arginine–treated MDA-MB-231 and MDA-MB-468 xenografts. (**D**) Significantly changed metabolites belonging to the glycolysis pathway and TCA cycle in vehicle- versus L-arginine–treated MDA-MB-231 and MDA-MB-468 xenografts. (**E**) NAD$^+$ levels in vehicle- versus L-arginine–treated MDA-MB-231 and MDA-MB-468 xenografts. (**F**) ATP:ADP and (**G**) ATP:AMP ratios in vehicle- versus L-arginine–treated MDA-MB-231 and MDA-MB-468 xenografts. *P_{adj} < 0.01, **P_{adj} < 0.001, ***P_{adj} < 0.0001, and ****P_{adj} < 0.00001.

abundance of 92 and 89 metabolites in MDA-MB-231 and MDA-MB-468 tumors, respectively (Fig. 3B). Arginine was among the increased metabolites in the L-arginine–treated mice ($P_{adj} < 0.0001$ for both; Fig. 3C). Although this dose was enough to increase arginine content in the tumors, there was evidence of certain degree of metabolization by arginase as suggested by increased levels of ornithine and argininosuccinate (fig. S3). Similar to BM patients, L-arginine also significantly reduced the levels of lactate in the TNBC xenografts (Fig. 3D).

Specific analysis of the glycolytic pathway indicated reduced levels of metabolites downstream of glyceraldehyde-3-phosphate dehydrogenase (GAPDH) (Fig. 3D), suggesting a reduced activity of this enzyme. Reduced GAPDH activity can be a direct consequence of NO-dependent GAPDH S-nitrosylation (38–40). In addition, the reduction in nicotinamide adenine dinucleotide (NAD⁺) (Fig. 3E) may have also contributed to decreased GAPDH activity (40). L-Arginine also decreased some of the tricarboxylic acid (TCA) cycle metabolites (Fig. 3D) and ultimately affected energy production, as evidenced by reduced adenosine 5′-triphosphate:adenosine 5′-monophosphate (ATP:AMP) and ATP:adenosine 5′-diphosphate (ATP:ADP) ratios (Fig. 3, F and G). Overall, these data indicate that the reduction in the lactatogenic phenotype of tumors upon L-arginine administration to patients and animal models is associated to a more extended metabolic suppression.

L-Arginine suppression of tumor metabolism occurs in a NOS2-dependent manner

Because NOS2 is the main NOS isoform expressed by cancer cells (20), we assessed its contribution to the metabolic effect of L-arginine. Cancer cell cultures are exposed to high concentrations of nutrients, including arginine, making it challenging to directly translate doses and timing from in vivo experiments. Thus, we first identified the concentration of L-arginine that decreases lactate production in cells with a magnitude like that observed in BM patients and animal models. We exposed MDA-MB-231 and MDA-MB-231-BrM2 cells to several concentrations of L-arginine for 1 hour and measured extracellular lactate levels. We observed a significant reduction in lactate accumulation in both cell lines at 10 and 50 mM L-arginine (Fig. 4A). L-Arginine (50 mM) induced a more pronounced effect on lactate levels without inducing cell death, and this dose was used in subsequent experiments. We then exposed TNBC cells MDA-MB-231 and MDA-MB-468 to L-arginine for 1 hour alone or in the presence of the specific NOS2 inhibitor 1400W (41) and performed a metabolomic analysis. Principal components analysis revealed that exposure to L-arginine exerts a global effect on the metabolism of cancer cells that was to a great extent reverted by the NOS2 inhibitor (Fig. 4, B and C). Analyses of specific metabolites revealed that L-arginine affects the glycolytic pathway and the TCA cycle in a manner similar to what was observed in the TNBC xenografts for both cell lines (Fig. 4, D and E; fig. S4A; and table S3). Furthermore, we observed a similar reduction in NAD⁺ and in the ATP:AMP ratio upon L-arginine (Fig. 4, D and E; fig. S4A; and table S3). Notably, these metabolic effects were largely rescued by pretreatment with the NOS2 inhibitor (Fig. 4, D and E; fig. S4A; and table S3). Because in our clinical trial we used the reduction in tumor lactate as the metabolic readout for the L-arginine effect, we determined whether NOS2 mediated this effect using an extended panel of TNBC and NSCLC cell lines. Thus, we exposed cancer cells to L-arginine for 1 hour alone or in combination with the NOS2 inhibitor 1400W

and measured the extracellular lactate content. Inhibition of NOS2 was sufficient to rescue the L-arginine–induced lactate reduction in all cell lines tested (Fig. 4F).

Our in vivo and in vitro metabolomic analyses favored a scenario in which lactate reduction was a consequence of interference in the glycolytic pathway, rather than increased aerobic use of glucose. To experimentally support this notion, we measured the effect L-arginine on mitochondrial respiration in MDA-MB-231 cells. We found that L-arginine did not increase the oxygen consumption rate (OCR) upon treatment (Fig. 4G), and moreover, there was a mild decrease in the OCR. Accordingly, there were not significant differences in the consumption of glucose and glutamine in MDA-MB-231 cells treated with L-arginine for 1 hour (versus D-arginine; fig. S4B).

Mitochondria and glycolysis are two major sources of ATP in cancer cells, and sustained depletion of ATP can lead to cell death. We thus measured in real time the ATP production in MDA-MB-231 and MDA-MB-231-BrM2 cells upon L-arginine administration. We observed a significant reduction in ATP content as soon as 10 min after L-arginine treatment, an effect that was followed by a steady but slow recovery (Fig. 4H). L-Arginine did not induce cell death during this experiment (Fig. 4H), indicating that ATP depletion is transient and insufficient to trigger substantial necrosis in these cell lines. However, transient but biological relevant changes in ATP:AMP ratio can induce signaling-dependent compensatory mechanisms. We thus investigated the activation of the main cellular ATP:AMP sensor AMPK (AMP-activated protein kinase) in these conditions. We found an increase in AMPK phosphorylation in MDA-MB-231 and MDA-MB-231-BrM2 cells as soon as 10 min after L-arginine administration (Fig. 4I), mirroring cellular ATP levels. Activation of AMPK led to phosphorylation and inactivation of the key regulator of fatty acid synthesis acetyl–coenzyme A carboxylase 1 (ACC1) (Fig. 4I). Using our extended panel of cancer cell lines, we found that ATP levels were partially rescued by a NOS2 inhibitor at early and late time points (fig. S4C). These data demonstrated that the metabolic suppression induced by L-arginine is largely NOS2 mediated and, although profound, is of transient nature.

L-Arginine exposure results in NOS2-dependent GAPDH nitrosylation and PARP hyperactivation

Our findings suggest that the metabolic effect of L-arginine is likely secondary to NO-dependent changes in the activity of glycolytic enzymes. Exposure of MDA-MB-231 and MDA-MB-231-BrM2 cells to L-arginine induced NO production as soon as 15 min after treatment that lasted for at least 55 min (fig. S5, A and B). The biological effects of NO are mediated by the generation of reactive nitrogen species (RNS), among which peroxynitrite that can modulate protein activity by S-nitrosylation (42). We therefore measured the production of peroxynitrite in cells by designing a competitive assay in which production of H_2O_2 was assessed over time following exposure to L-arginine, a cell-permeable superoxide dismutase 1 mimetic (SOD1^{mim}) compound, or both. We reasoned that arginine-induced NO and SOD1^{mim} would compete to react with superoxide, resulting in the production of peroxynitrite or H_2O_2, respectively. Accordingly, exposure to L-arginine significantly blunted the amount of H_2O_2 produced upon SOD1^{mim} addition, indicating a significant peroxynitrite production in MDA-MB-231 and MDA-MB-231-BrM2 cells by L-arginine (Fig. 5A). This increase in peroxynitrite in cancer cells was consequential as it was followed by extensive proteome S-nitrosylation in MDA-MB-231 cells (Fig. 5B). Using our extended panel of cell lines,
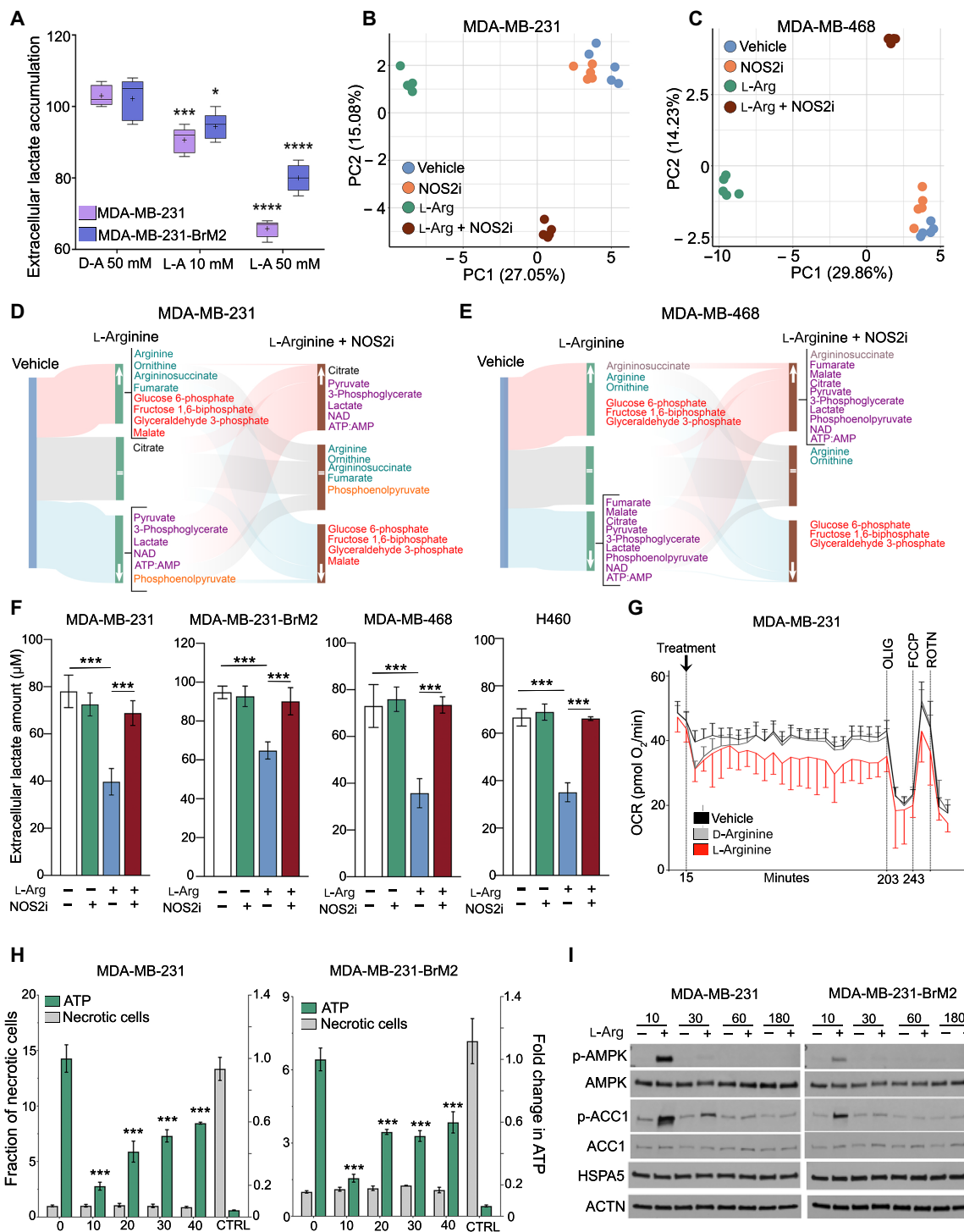
Fig. 4. L-Arginine suppression of tumor metabolism occurs in a NOS2-dependent manner. (**A**) Extracellular lactate concentration in MDA-MB-231 and MDA-MB-231-BrM2 cells treated for 60 min with D-arginine (as control) or L-arginine at the indicated concentrations. (**B** and **C**) Principal components (PC) analyses of the metabolome of MDA-MB-231 and MDA-MB-468 cells treated in vitro with vehicle, NOS2 inhibitor 1400W, L-arginine, or their combination. (**D** and **E**) Sankey plots depicting statistically significant metabolic changes exerted by L-arginine alone or in combination with the NOS2 inhibitor 1400W in MDA-MB-231 and MDA-MB-468 cell lines. Data compared to vehicle. Selected metabolites are indicated. The color pattern of metabolites indicates similar changes. (**F**) Extracellular lactate concentration in a panel of TNBC and NSCLC cell lines exposed to L-arginine alone or in combination with the NOS2 inhibitor 1400W. (**G**) Oxygen consumption rate (OCR) in MDA-MB-231 cells exposed to vehicle (black), D-arginine (gray), or L-arginine (red) for the indicated times. FCCP, carbonyl cyanide p-trifluoromethoxyphenylhydrazone; OLIG, oligomycin; ROTN, rotenone. (**H**) Total cellular ATP levels (right x axis) and cell necrosis (left x axis) in MDA-MB-231 and MDA-MB-231-BrM2 cells treated with L-arginine for the indicated time points (y axis, in minutes). Cyclophosphamide was used as a positive control for cell necrosis (CTRL). (**I**) Total and phosphorylated levels of AMPK and its target ACC1 in MDA-MB-231 and MDA-MB-231-BrM2 cells treated with L-arginine for the indicated time points (in minutes). HSPA5 and actin were used as controls. *$P < 0.01$, **$P < 0.001$, and ***$P < 0.0001$.
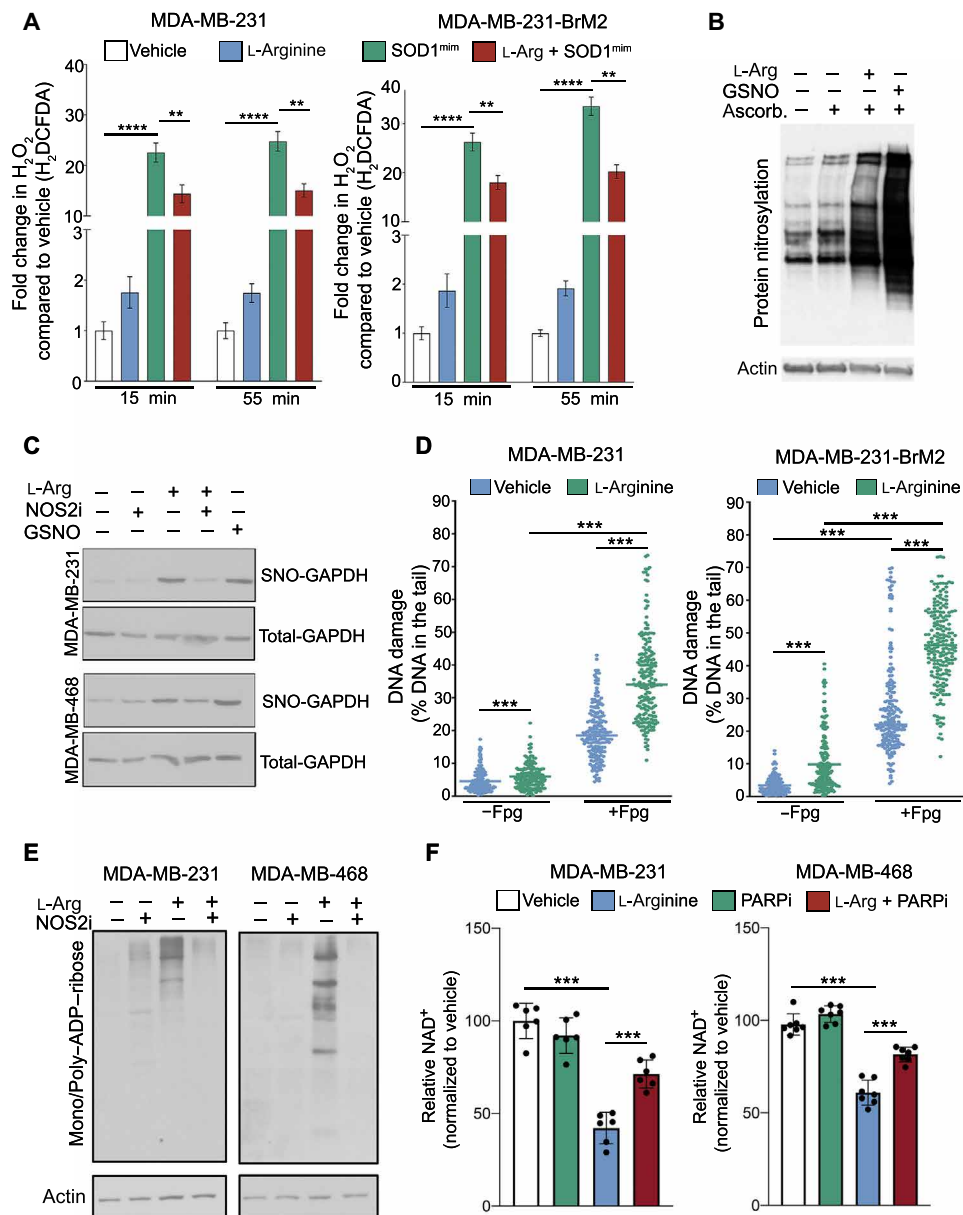
Fig. 5. L-Arginine generates peroxynitrate, GAPDH nitrosylation, and protein ADP-ribosylation. (**A**) Peroxynitrate levels in MDA-MB-231 and MDA-MB-231-BrM2 cells treated with vehicle, L-arginine, the SOD mimetic tempol (SOD1^{mim}), or the combination of L-arginine and SOD1^{mim} for 15 and 55 min. (**B**) Total protein nitrosylation in MDA-MB-231 cells exposed to L-arginine for 60 min. GSNO was used as a positive control. (**C**) SNO-GAPDH (and total GAPDH) in MDA-MB-231 and MDA-MB-468 cells exposed for 60 min to L-arginine alone or in combination with the NOS2 inhibitor 1400W. GSNO was used as a positive control. (**D**) DNA damage levels assessed by comet assay in MDA-MB-231 and MDA-MB-231-BrM2 cells exposed to vehicle or L-arginine for 60 min with and without Fpg. (**E**) Total mono– and poly–ADP-ribosylated proteins in MDA-MB-231 and MDA-MB-468 cells exposed to L-arginine alone or in combination with the NOS2 inhibitor 1400W. (**F**) NAD$^+$ levels in MDA-MB-231 and MDA-MB-468 cells exposed to L-arginine alone or in combination with the PARP inhibitor olaparib. **$P < 0.001$ and ***$P < 0.0001$.

we demonstrated that the global proteome S-nitrosylation was blunted by the NOS2 inhibitor 1400W (fig. S5C). Because our metabolic data showed impaired glycolysis and GAPDH can be transiently inhibited by S-nitrosylation (*40*), we determined whether this effect was occurring in our cells. We exposed MDA-MB-231 and MDA-MB-468 cells to L-arginine alone or in combination with the NOS2 inhibitor 1400W and determined S-nitrosylated (SNO)–GAPDH by the biotin switch assay. The NO donor *S*-nitrosoglutathione (GSNO) was used as a positive control. We found an increase in SNO-GAPDH levels

in both cell lines upon L-arginine administration (Fig. 5C). This effect was rescued by the concomitant administration of the NOS2 inhibitor (Fig. 5C).

The NAD$^+$ depletion that we observed in our metabolic studies can also inhibit the activity of GAPDH, reinforcing the inhibition caused by S-nitrosylation (*40*). Decreased levels of NAD$^+$ can be a consequence of PARP [poly(ADP-ribose) polymerase] hyperactivation secondary to a nitrosative DNA damage (*43*). We thus determined whether L-arginine induces DNA damage in MDA-MB-231 and

MDA-MB-231-BrM2 cells by the alkaline comet assay. Compared to vehicle, we observed a significant increase in DNA damage level in both cell lines treated with L-arginine for 1 hour (Fig. 5D). Such difference was even more evident when the endonuclease Fpg was used to detect oxidized bases in addition to DNA single-strand breaks, double-strand breaks, and alkali-labile sites (Fig. 5D), suggesting a high level of nitrosative damage. Next, under the same experimental conditions, we determined PARP hyperactivation in MDA-MB-231 and MDA-MB-468 cells by a proteome mono– and poly–ADP-ribosylation assay. L-Arginine resulted in PARP hyperactivation, an effect that was rescued by NOS2 inhibition (Fig. 5E). To determine whether PARP hyperactivation contributed to NAD^+ depletion, we exposed MDA-MB-231 and MDA-MB-468 cells to L-arginine or the PARP inhibitor olaparib, alone or in combination, and measured NAD^+ levels by a bioluminescence assay. Similar to what was observed in metabolomic studies (Fig. 3D), L-arginine induced a significant reduction in NAD^+ levels in both cell lines, an effect partially rescued by PARP inhibition (Fig. 5F). Overall, these data support a model in which the metabolic effects of L-arginine occur via NOS2-dependent generation of NO and subsequent induction of SNO-GAPDH and DNA damage with PARP hyperactivation.

L-Arginine decreases the DNA damage repair capacity of cancer cells

Although the transient metabolic suppression induced by L-arginine may be insufficient to cause cell death, it could be critical for DNA repair in cells sublethally damaged upon radiation. To test this notion, we treated our panel of cell lines to either vehicle or L-arginine for 1 hour and then exposed them to increasing doses of gamma radiation (1 to 6 Gy) followed by a colony-forming assay. As expected, L-arginine alone did not affect colony formation in any of the cell lines analyzed; however, L-arginine effectively sensitized cancer cells to radiation treatment with SER-2Gy (sensitizer enhancement ratio at 2 Gy) between 1.44 and 2.09 across all the cell lines (Fig. 6A). The radiosensitization effect of L-arginine was maintained between fractions of radiation administered 4 hours apart (fig. S6). As we showed for the metabolic effects of L-arginine, its radiosensitization effect was also rescued in all the cell lines tested by the administration of the NOS2 inhibitor (Fig. 6B).

The metabolic suppression induced by L-arginine may impair the synthesis of intermediates required for DNA repair. We thus measured the synthesis of DNA in MDA-MB-231-BrM2 cells exposed to L-arginine for 1 hour alone or in the presence of the NOS inhibitor N_G-monomethyl-L-arginine (L-NMMA). We found that L-arginine significantly decreased DNA synthesis and that this effect was rescued by L-NMMA (Fig. 7A). To measure how this will affect the capacity of cancer cells to repair double-strand breaks, we first exposed MDA-MB-231-BrM2 cells to vehicle or L-arginine for 1 hour followed by ionizing radiation and determined γH2AX-53BP1 foci formation as a marker of DNA double-strand breaks. As expected, ionizing radiation induced γH2AX-53BP1 foci in these cells, an effect increased by pretreatment with L-arginine (Fig. 7B). L-Arginine alone did not induce detectable foci in these cells. Then, using the same experimental conditions, we conducted an alkaline comet assay to assess the capacity of cells for DNA repair. The level of unrepaired DNA was quantified at 30 min and 4 hours after irradiation. We found that, compared to vehicle, cells pretreated with L-arginine for 1 hour
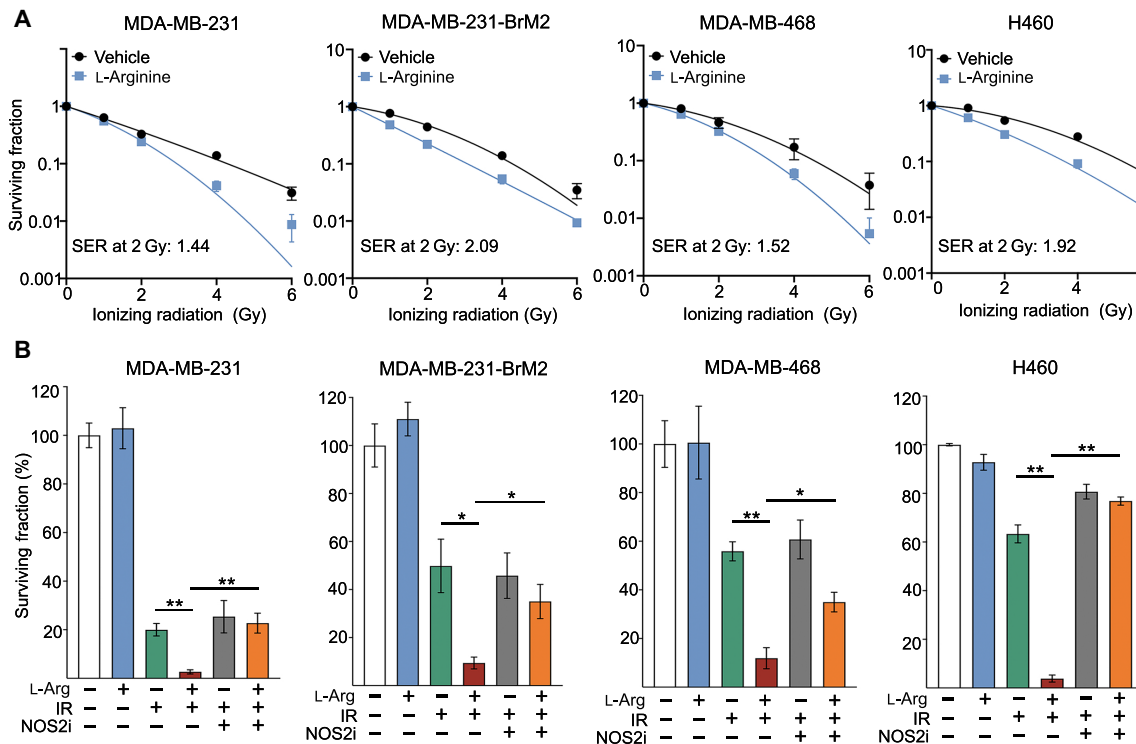
Fig. 6. L-Arginine radiosensitizes cancer cells in a NOS2-dependent manner. (**A**) Dose response curves of MDA-MB-231, MDA-MB-231-BrM2, MDA-MB-468, and H460 cells exposed to L-arginine for 60 min followed by a dose range of ionizing radiation. (**B**) Surviving fraction of MDA-MB-231, MDA-MB-231-BrM2, MDA-MB-468, and H460 cells exposed to vehicle or L-arginine for 60 min followed by 2-Gy ionizing radiation with or without the NOS2 inhibitor 1400W. *$P < 0.01$, **$P < 0.001$, and ***$P < 0.0001$.
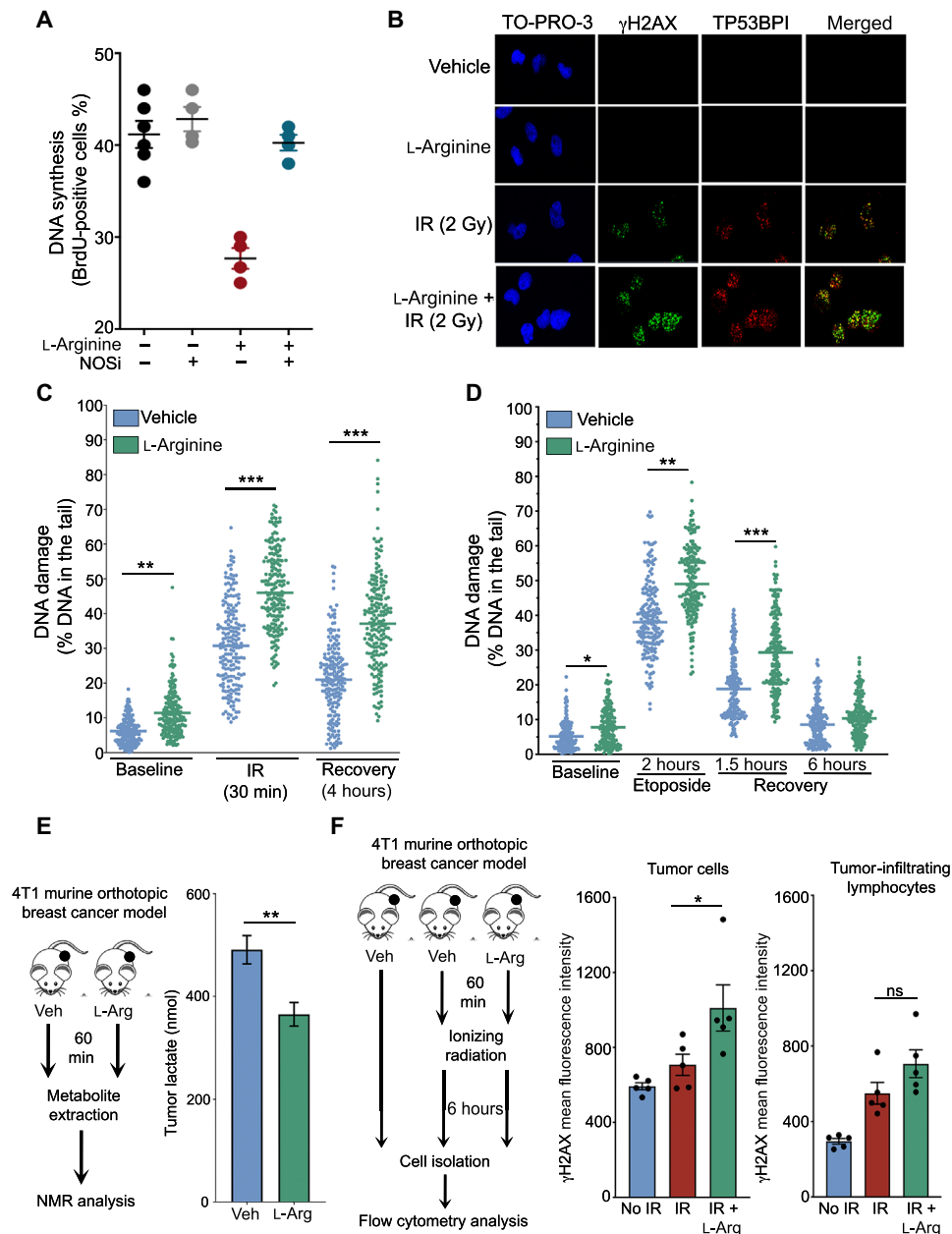
Fig. 7. L-Arginine decreases the DNA damage repair capacity of cancer cells. (**A**) DNA synthesis capacity determined by 5-bromo-2′-deoxyuridine (BrdU) incorporation in MDA-MB-231 cells exposed to vehicle or L-arginine for 60 min with or without the NOS inhibitor L-NMMA. (**B**) Representative images of nuclear γH2AX and 53BP1 foci in MDA-MB-231-BrM2 cells exposed to vehicle, L-arginine, ionizing radiation, or the combination. (**C**) DNA damage levels assessed by comet assay in MDA-MB-231-BrM2 cells exposed to vehicle or L-arginine for 60 min followed by ionizing radiation (4 Gy). DNA damage was assessed at 60 min following L-arginine administration (baseline, before irradiation) and at 30 min and 4 hours following irradiation. (**D**) DNA damage levels in MDA-MB-231-BrM2 cells exposed to vehicle or L-arginine for 1 hour followed by etoposide for 2 hours. DNA damage was assessed by comet assay at 1 hour after vehicle or L-arginine administration, at 2 hours after etoposide treatment, and at 1.5 and 6 hours after drug washing (recovery). (**E**) Intratumor lactate concentration in the murine 4T1 TNBC orthotopic model. Mice were treated with vehicle or a mouse-equivalent dose of L-arginine administered by oral gavage, and tumor lactate content was measured after 60 min by nuclear magnetic resonance (NMR). (**F**) Experimental design (left) to determine γH2AX levels by flow cytometry in tumor cells (middle) and CD45^{+} tumor-associated lymphocytes (right) isolated from the murine 4T1 TNBC orthotopic model. Mice were treated with vehicle or a mouse-equivalent dose of L-arginine followed by ionizing radiation (2 Gy). Data are shown in viable cells (cleaved caspase-3[NEG]). *P < 0.01, **P < 0.001, and ***P < 0.0001. ns, not significant.

displayed significantly higher levels of residual unrepaired DNA damage at both time points following ionizing radiation (Fig. 7C). Similarly, pretreatment with L-arginine for 1 hour (versus vehicle) increased the level of unrepaired DNA when the chemotherapeutic agent etoposide was used as a source of DNA damage (Fig. 7D).

To evaluate the effect of L-arginine in decreasing the DNA repair capacity in vivo, we used the murine model of aggressive TNBC 4T1 (*44*). First, we determined whether the decrease in the lactatogenic phenotype induced by oral L-arginine as we observed in BM patients was recapitulated in this model. Once orthotopic TNBC 4T1 tumors

were fully established, mice were randomized to vehicle ($n = 5$) or to a mouse-equivalent oral dose of L-arginine ($n = 5$). After 1 hour of L-arginine or vehicle administration, tumors were harvested and processed to measure lactate concentration via nuclear magnetic resonance (NMR). As observed in BM patients, L-arginine significantly reduced the lactate content of these tumors (Fig. 7E). To evaluate the capacity of cells to repair DNA damage in these conditions, we measured γH2AX foci by flow cytometry. Mice orthotopically implanted with 4T1 were randomized to receive vehicle ($n = 5$), vehicle for 1 hour followed by irradiation ($n = 5$), or mouse-equivalent dose of L-arginine for 1 hour followed by irradiation ($n = 5$; Fig. 7F). After 6 hours following 2-Gy ionizing radiation, tumors were harvested, and DNA damage levels were assessed by quantification of γH2AX in isolated mCherry$^+$/CD45$^-$ tumor cells. Frank apoptotic cells positive for cleaved caspase-3 were excluded from the analysis. In vehicle-treated mice, cancer cells from irradiated mice displayed higher levels of γH2AX compared to nonirradiated mice, indicating residual unrepaired DNA damage (Fig. 7F). The fraction of cancer cells sustaining unrepaired DNA damage was significantly higher in mice receiving L-arginine (versus irradiation alone, $P < 0.05$; Fig. 7F). At this time point, these cells are likely sublethally damaged because the differences in γH2AX levels were not due to increased apoptosis as determined by cleaved caspase-3 (fig. S7). To evaluate whether noncancer cells are equally susceptible to cancer cells to the radiosensitizing effect of L-arginine, we measured γH2AX levels in tumor-infiltrating lymphocytes mCherry$^-$/CD45$^+$. While irradiation resulted in increased levels of DNA damage, the effect of adding L-arginine was negligible in these cells (Fig. 7F). Overall, these data indicate that, at clinically relevant doses, L-arginine impairs DNA damage repair preferentially in cancer cells.

DISCUSSION

We report the effect of oral L-arginine as a radiosensitizer in solid tumor patients harboring BM. We identified a dose of L-arginine that was well tolerated and achieved better local disease control compared to placebo in combination with bidaily radiation administration. Functional imaging analyses revealed a marked reduction in lactate concentration in BM of patients after L-arginine administration, suggesting a potential metabolic effect on cancer cells. Using preclinical models, we found that this reduction in the lactatogenic phenotype of cancer cells was part of an extended sublethal metabolic suppression associated with transient energy depletion. This effect was mechanistically linked to metabolization of L-arginine to produce NO through the isoform NOS2 that is expressed in cancer cells. We determined that the ATP depletion was an ultimate consequence of decreased glucose catabolism. Cells with high glycolytic capacity, like most cancer cells, could partially compensate a decrease in respiration-generated ATP with an increase in the glycolytic flux (45). However, as we demonstrated in our models, NO can induce S-nitrosylation of the enzymatic site of GAPDH preventing such compensation (40). Furthermore, our metabolomic analysis suggested that depletion of NAD$^+$ could be an additional factor contributing to glycolysis inhibition (46). We showed that, in cancer cells treated with L-arginine, NAD$^+$ depletion is partially a consequence of PARP hyperactivation due to the DNA damage induced by NO metabolites (47). In addition, increased lipid oxidation also alters the NAD:NADH ratio particularly when cells cannot recover it from pyruvate (46).

At the molecular level, we found that L-arginine impaired cancer cell's ability to repair DNA damage, likely explaining the

radiosensitization observed in BM patients. Impaired DNA damage repair may be secondary to the transient metabolic suppression, as we observed that L-arginine limited the capacity of cancer cells to produce the intermediates required for DNA synthesis. Additional mechanisms that may have contributed to the observed impairment in DNA damage repair included the S-nitrosylation of DNA damage repair proteins (48) and/or the generation of low-reparability complex DNA lesions (49) due to the association of ionizing radiation with nitrosative damage.

We speculate that the transient effect of L-arginine on cancer cell metabolism has the potential advantage to avoid a complete metabolic reprogramming and subsequent emerging of counter-regulatory mechanisms that could adapt cells to L-arginine administration. The relative gain in the anticancer effect of radiation with L-arginine administration was maintained between fractions of radiation administered 4 hours apart. In patients, together with minimizing post-radiation hypoxia, this could have resulted in lower toxicity and likely higher efficacy over less fractionated regimens. Nevertheless, the contribution of L-arginine administration in relation to fractionation modalities has not been fully explored in our studies. Furthermore, because L-arginine was administered only for the duration of the radiation treatment, it is unlikely that it would have exerted any systemic pro-inflammatory effects.

Overall, our mechanistic studies indicate that the radiosensitization effect of L-arginine observed in patients is mostly induced in a cancer cell–intrinsic manner. This agrees with early reports showing growth arrest in cancer cell lines supplemented with L-arginine (50). On the contrary, other groups reported a radiosensitizing effect of arginine deprivation therapies (ADIs) in other cancer types (51–53). However, the radiosensitizing effect of ADI seems to be largely dependent on whether cancer cells are auxotrophic for arginine (53). Furthermore, most of these studies only used in vitro models, thus excluding the potential contribution of cellular-extrinsic mechanisms. We observed a relatively stronger radiosensitizing effect in patients compared to our in vitro models. In this regard, L-arginine administration not only decreased the lactatogenic phenotype of BM but also may have improved the tumor hemodynamics. In contrast to the physiological vasculature, the vascular morphology of BM is highly irregular, presenting collapsed vessels and sinusoid-like capillaries that may result in the coexistence of over-, normal-, and under-perfused regions within the same tumor (54), thus creating hypoxic and radioresistant areas. We observed that L-arginine administration may had homogenized the microvasculature of BM, an effect that could have improved BM oxygenation, thus promoting radiosensitization (55). This could represent an advantage of L-arginine over pharmacological NO donors and related molecules that tend to acutely modify the systemic hemodynamic parameters potentially lowering the TBF and increasing their hypoxic fraction (17).

An additional factor potentially contributing to the overall antineoplastic effect of L-arginine is the resultant immune activation. Early data suggested that subcutaneous L-arginine administration inhibits the growth of rat mammary tumors (56). Furthermore, we observed that L-arginine administration does not alter the amount of radiation-induced DNA damage in tumor-infiltrating lymphocytes, indicating that our approach is unlikely to be detrimental for immune cell activity. On the contrary, recent data demonstrated that oral L-arginine administration in murine cancer models results in improvement of metabolic fitness of T cells that are crucial for antitumor responses (57). Although less likely to play a role in

advanced cancer patients, the combination of antitumor immuno-therapy with the radiosensitizing properties of L-arginine deserves further study. The administration of L-arginine before radiation thera-py reverses radiation-induced T cell– and B cell–dependent immune dysfunction in mice (58). Although the mechanism is not fully elu-cidated, we speculate that the decrease in lactate production from cancer cells, as we demonstrated here was induced by L-arginine, may have also contributed to improve the antineoplastic activity of tumor-infiltrating lymphocytes (59). Regardless of the role of lactate in the TME, our results demonstrating the impact of L-arginine administra-tion on the lactatogenic phenotype of BM and its association with acquisition of radiation sensitization suggest that assessment of tumor lactate variation with MRS could be used as a noninvasive pharmaco-dynamic biomarker for patient selection.

In summary, we showed that L-arginine administration directly affects the metabolism of cancer cells affecting their capacity of sur-vival upon sublethal DNA damage, a mechanism that we therapeu-tically capitalized to increase the response to radiation therapy for patients with BM.

PATIENTS AND METHODS
Clinical trial
A randomized clinical trial of placebo versus L-arginine followed by whole-brain irradiation in patients with pathology-confirmed diag-nostic of solid cancer and unresectable BM was approved by The Angel H. Roffo Committees for Clinical Investigation and Ethics (registration: NCT02844387). Eligibility criteria are as follows: Karnofsky performance score ≥ 70, presence or absence of extracranial metas-tases, presence or absence of controlled primary tumor, measurable brain lesion/s by contrast-enhanced computed tomography (CT) scan or MRI scan, no previous treatment for BM, absolute granulo-cyte count $\geq 2000/mm^3$, hemoglobin ≥ 9 g/liter (patients with lower levels were transfused before the randomization), normal renal func-tion (serum creatinine <1.5 mg/dl and 24-hour creatinine clearance >60 ml/min), and normal hepatic function (aspartate aminotrans-ferase and alanine aminotransferase <2.5 times the upper limit of normal). All patients submitted written informed consent.

Treatment
L-Arginine was administered at 10 g per dose 1 hour before each frac-tion of radiation. L-Arginine monohydrochloride was purchased from the market (Drogueria Saporiti, Buenos Aires, Argentina) and pre-pared by the hospital compounding pharmacy as lemon-flavoring aqueous suspension to be reconstituted immediately before use to a final volume of 200 ml per dose. Placebo consisted of 200 ml of lemon-flavoring suspension prepared in the same manner as the active com-pound. To prevent nausea and vomiting, methoclopramide was administered 15 min before L-arginine or placebo. The whole brain was treated by two lateral fields to a total dose of 32 Gy adminis-tered in 20 fractions of 1.6 Gy bidaily with a 6-hour interval between treatments for 10 days, followed by a 22.4-Gy boost over the evident lesions with the same fractionation schedule for 7 days. All patients were irradiated with 6-MV photons. The dose to organs at risk (i.e., spinal cord, optic chiasm, and brain stem) was limited to 40 Gy. Dexamethasone was used at the lowest dosage required to maintain patients at their maximum level of comfort and function. For patients with no previous usage, concurrent administration of dexametha-sone was allowed at a dose of 4.5 mg/day orally with a slow reduction after radiotherapy. For patients with previous usage, dexamethasone

dosage was decreased until symptoms increased or became apparent, and then increased until they subside. For deteriorating patients, rescue with dexamethasone (orally or intravenous) was allowed and clinically recorded. All patients were followed up without further treatment.

Response evaluation and adverse event reporting
Efficacy was assessed by response rate considering radiological, symptomatic, and overall responses following the RECIST (Response Evaluation Criteria in Solid Tumors) guidelines and by determining PFS, neurological PFS (NPFS), and OS. Patients were observed until death or were censored at the time that the study was closed for this analysis. PFS, NPFS, and OS were calculated from day 1 of radiation therapy to documented disease progression or death, documented neurological progression or death, and death, respectively. The in-vestigators' determinations of tumor response and disease progression were used in the data analysis. The U.S. National Cancer Institute Common Terminology Criteria for Adverse Events (CTCAE) was used to score treatment toxicity.

Metabolic and vascular profiling of BM
Lactate in BM was determined by MRS baseline and, followed by a contrasting agent washout period of 24 hours, after 1 hour of oral ad-ministration of 10 g of L-arginine or placebo. MRS data were obtained by using a double spin-echo point-resolved spectroscopy (PRESS) sequence with one-pulse water signal suppression mainly from metabolically active areas of the lesions while avoiding contamination from scalp fat. Appropriate automatic shimming and water suppres-sion were achieved by using 4- to 8-Hz linewidth and 1-kHz spectral width. Spectroscopic data from cubic volumes of 1.5 cm × 1.5 cm × 1.5 cm to 2 cm × 2 cm × 3 cm were obtained by using the PRESS sequence with 1500/135 ms, 128 to 256 averages, 1024 data points, and 4000-Hz spectrum width. In most examinations, a voxel size of 2 cm × 2 cm × 2 cm was used. The time domain signal intensity was apodized and processed to remove the residual water signal. Post-processing of the MRS data consisted of frequency shift and phase and linear baseline corrections after Fourier transformation. In most cases, these processes were automatic, but where spectra appeared distorted, manual processing was used, particularly for phase and baseline corrections. Frequency domain curve was fitted to Gaussian line shape by using the software provided by the manufacturer to de-fine N-acetylaspartate, choline-containing components, and creatine-phosphocreatine peaks. Lactate peak was calculated at 1.35 parts per million (an inverted ß-methyl doublet). The lactate assignment was made based on an inverted doublet due to J coupling of lactate-bound protons at a echo time (TE) of 135 ms. Lactate values were calculated automatically from the area under the peak by using the standard commercial software program provided by the manufacturer. BM vascularization was estimated by perfusion-weighted MRI with an intravascular gadolinium contrast bolus (0.1 mmol/kg at 5 ml/s fol-lowed by saline flush) using a GE Signa scanner (GE Healthcare). The following parameters were determined: TBF (volume of blood pass-ing through a given amount of tissue per minute), TBV (volume of blood in each amount of tissue), signal time to peak (STP), and mean transit time (MTT) of the contrast bolus. A relative TBV map was derived on a pixel-by-pixel basis from the dynamic image sets using the manufacturer's software. Parameters were obtained from whole lesions and from normal white/gray matter used for normalization. Glucose uptake was determined using fludeoxyglucose (^{18}F) PET/CT scanning using a Discovery STE16 machine (GE Healthcare). Patients

were scanned after 4-hour fasting with normal glucose blood levels. Baseline and post–L-arginine studies were done 24 hours apart.

Immunohistochemistry

Immunohistochemistry was performed following standard pathology protocols in deparaffinized BM tissues from deidentified patients using mouse monoclonal anti-NOS2 (C-11) and mouse monoclonal anti-NOS3 (A-9) both from Santa Cruz Biotechnology. Evaluation and scoring were independently made by at least two investigators. Percentage of positive tumor cells and intensity of staining (by using an ad hoc scale from 1 to 4) were used to determine the total score.

Cell lines and compounds

The TNBC cell lines MDA-MB-231 and MDA-MB-468 and the NSCLC cell line H460 were purchased from the American Type Culture Collection (ATCC). The MDA-MB-231-BrM2 cell line was obtained from J. Massague (Memorial Sloan Kettering Cancer Center, New York, NY). The mouse TNBC cell line 4T1 was obtained from Vivek Mittal (Weill Cornell Medicine, New York, NY). Identification was done once a year by genotyping, and mycoplasma was tested quarterly by polymerase chain reaction (PCR). Cells were cultured in Dulbecco's modified Eagle's medium (DMEM) (human and murine TNBC cells) or RPMI 1640 medium (NSCLC cells) supplemented with fetal calf serum and antibiotics (penicillin and streptomycin) or with a low-buffered DMEM medium with no Hepes and supplemented with 1 mM phosphate buffer (pH 7.2) in certain experiments. L-Arginine and D-arginine were purchased from Sigma-Aldrich and dissolved in RPMI 1640 (adjusting the final pH to 6.8 to 7.2). The competitive NOS inhibitor N^G-monomethyl-L-arginine and the NOS2 selective inhibitor 1400W dihydrochloride were purchased from Sigma Chemical and Enzo Life Science, respectively. Compound solutions were prepared fresh for each experiment.

NOS2 expression in breast cancer cells

Cells were exposed to hypoxia (1% O_2) or IL-6 (40 nM) for 3 hours, after which total RNA was isolated by TRIzol reagent (Invitrogen). One microgram of RNA for each condition was converted to complementary DNA (cDNA) using the Verso cDNA Synthesis Kit (Thermo Fisher Scientific) according to the manufacturer's protocol. Quantitative reverse transcription PCR was carried out in 384-well plates using the 7900HT Fast Real-Time PCR System (Applied Biosystems). A dissociation curve analysis was performed for each sample to verify PCR specificity, and no template samples were used as negative control. NOS2 messenger RNA fold change was calculated by the $\Delta\Delta C_t$ method using RPLP0 as an internal control and vehicle-treated cells as a calibrator.

Mice experiments

All animal work was conducted in accordance with a protocol approved by the Institutional Animal Care and Use Committee at Weill Cornell Medical College. In these studies, the mouse equivalent dose (MED) of the human dose of 10 g of L-arginine was considered as 1.75 g/kg (corrected for body surface area). Pharmacological grade of L-arginine monohydrochloride was purchased from Sigma-Aldrich and reconstituted in aqueous suspension with pH adjusted to 6.5 to 7.0 immediately before administration. For studies using human xenografts, 6- to 8-week-old female severe combined immunodeficient (SCID) mice were subcutaneously injected in the flank with 10^7 human breast cancer MDA-MB-231 or MDA-MB-468 cells. When tumors reached a palpable size (approximately 75 to 100 mm^3), mice were

randomized in two treatment arms to receive one dose of either vehicle ($n = 5$) or a MED of L-arginine ($n = 5$) via oral gavage. After 1 hour, mice were euthanized, and tumors were harvested and processed for metabolomic analysis. For studies using murine breast cancer model, 6- to 8-week-old female BALB/c mice were injected in the mammary fat pad with 5×10^5 4T1 cells expressing mCherry. For intratumor lactate content, mice were randomized to receive vehicle ($n = 5$) or a MED of L-arginine ($n = 5$) via oral gavage and tumors were harvested after 60 min. Metabolite extraction from 100 mg of wet tissue and subsequent NMR analysis were performed as previously described (60). For DNA damage assessment, mice ($n = 15$) were first randomized to receive vehicle ($n = 10$) or a MED of L-arginine ($n = 5$) via oral gavage; vehicle-treated mice were further randomized to no irradiation arm ($n = 5$) or ionizing radiation arm ($n = 5$). After 60 min following vehicle ($n = 5$) or L-arginine ($n = 5$) administration, mice were exposed to 2 Gy of gamma radiation. After 6 hours, tumors were harvested and processed for downstream analysis.

Metabolomic assays

For xenograft metabolomics, we processed 100 mg of tissue per condition by grinding in liquid nitrogen. Polar metabolites were extracted by adding 500 µl of cold high-performance liquid chromatography (HPLC)–grade 80% methanol and subsequent incubation at −80°C for 4 hours. Samples were then spun at 14,000 relative centrifuge force (rcf) for 20 min at 4°C, and the supernatant was concentrated by using a speed vacuum. For cancer cell metabolomics, 2×10^6 MDA-MB-231 and MDA-MB-468 cells were exposed to vehicle or the NOS2 inhibitor 1400W (50 µM) for 1 hour; subsequently, cells from each group were exposed to vehicle or 50 mM L-arginine for 1 hour and polar metabolite was extracted as mentioned above. Polar metabolites were detected by ultrahigh-performance liquid-phase chromatography coupled with tandem mass spectrometry. Liquid chromatography/mass spectrometry (LC/MC), data extraction, quality control, and compound identification were performed by WCM Proteomic and Metabolomic Core Facility. For all metabolomic assays, five biological replicates per conditions were used. Metabolites with more than 20% missing values and nonidentified metabolites were excluded. Data were quotient-normalized (61), and all metabolite concentrations were converted to log$_2$ before statistical analysis. Statistical analyses were performed in R 3.6.3 by using the maplet toolbox (https://github.com/krumsieklab/maplet). Treatment effects for each metabolite were assessed using paired t tests. False discovery rate (FDR) control according to Benjamini and Hochberg (62) was used to correct for multiple hypothesis testing.

Cellular lactate production

L-Lactate in the culture medium (serum-free low-buffered DMEM) of TNBC cells treated with vehicle or L-arginine (10 and 50 mM for 1 hour) alone or in combination with the NOS2 inhibitor 1400W (50 µM) was determined using an assay kit (BioVision, K607-100) following the manufacturer's instructions. Culture medium samples were filtered using a 10-kDa molecular weight spin filter (BioVision). Lactate concentration was derived from the colorimetric [optical density (OD) at 570 nm] measurement using a standard curve.

OCR and substrate consumption assay

OCR was measured by using the Seahorse XF96 Extracellular Flux Analyzer (Agilent). Briefly, cells were seeded on Cell-Tak (BD Biosciences) precoated XF96 plates, spun at 40g, and incubated

in an XF incubator without CO_2 for 25 min to ensure cell reattachment. Measurements were taken before the addition of any inhibitor (basal respiration) and after the sequential injection of 1 μM oligomycin (for ATP-linked respiration), 0.5 μM FCCP (carbonyl cyanide *p*-trifluoromethoxyphenylhydrazone) (for maximal respiration), and 1 μM rotenone/antimycin A (for nonmitochondrial oxygen consumption). Glucose and glutamine consumption was measured by using a BioProfile Basic analyzer (Nova Biomedical) according to the manufacturer's instructions. A well without cells and with the same medium under the same culture conditions was used as reference to estimate the glucose and glutamine consumed by cells.

ATP levels
ATP was determined using CellTiter-Glo (Promega) according to the manufacturer's protocol. Cells were seeded in triplicate for each condition and exposed to either vehicle, L-arginine (50 mM), or the NOS2 inhibitor 1400W (50 μM), alone or in combination, for the indicated times. The fraction of viable cells in each well was determined by CytoTox-ONE Homogeneous Membrane Integrity assay (Promega). Luminescence and fluorescence were measured using a Synergy4 microplate reader (BioTek).

NOS activity assay
The production of nitrite and nitrate was used to quantify the activity of NOS in lysates from cells grown in DMEM culture medium and treated with vehicle or L-arginine for 1 hour using an assay kit (NOS assay, BIOXYTECH) following the manufacturer's instructions. Cell lysates were prepared from flash-frozen cells in phosphate-buffered saline (PBS) buffer (pH 7.4) using mechanical disruption and filtered using a 10-kDa molecular weight spin filter (BioVision). Total nitroso compound concentration was derived from the colorimetric (OD at 540 nm) measurement using a standard curve and was used to calculate the enzyme activity (expressed as nmol/min per ml).

NO/RNS levels
Kinetic analysis of NO/RNS levels was performed by incubating the cells with 4-amino-5-methylamino-2′,7′-difluorofluorescein diacetate (5 μM) or 2′-7′-dichlorodihydrofluorescein diacetate (10 μM) for 30 min at 37C°. L-Arginine (50 mM), the competitive NOS inhibitor L-NMMA (200 μM), or the SOD mimetic Tempol (200 μM) was added to the medium after removal of the reactive probes. Fluorescence intensity was assessed at the indicated time points by using a Synergy4 microplate reader (BioTek).

Protein S-nitrosylation and biotin switch assay
Protein *S*-nitrosocysteine was detected after exposure to L-arginine (50 mM) by using a modified S-nitrosylation switch assay (Pierce) according to the manufacturer's protocol. Briefly, after cell lysis, unmodified cysteines were blocked with a sulfhydryl-reactive compound, while *S*-nitrosocysteine was reduced and irreversibly labeled. The amount of protein S-nitrosylation was then determined by immunoblotting. GSNO (200 μM) was used as a positive control. A negative control was generated by labeling sample without previous reduction of *S*-nitrosocysteine. GAPDH nitrosylation was detected by performing a standard biotin switch assay. Briefly, 7×10^6 cells were exposed to vehicle or the NOS2 inhibitor 1400W (50 μM) for 1 hour, and subsequently, cells from each group were exposed to 50 mM L-arginine for 1 hour. GSNO was used as a positive control. Cells were lysed in HEN buffer + 1% SDS (HENS) buffer, free cysteine thiols

were blocked with MMTS (methyl methanethiosulfonate; Thermo Fisher Scientific), and nitrosylated proteins were labeled with EZ-Link HPDP Biotin (Thermo Fisher Scientific). Labeled proteins were pulled down with neutravidin agarose beads (Thermo Fisher Scientific). Total GAPDH (input) and SNO-GAPDH (pull-down) were detected with an anti-mouse GAPDH antibody (MA1-16757, Invitrogen).

PARP activity assay
Breast cancer cells were exposed to vehicle or the NOS2 inhibitor 1400W (50 μM) for 1 hour, and subsequently, cells from each group were exposed to 50 mM L-arginine for 1 hour. Lysis buffer [40 mM Hepes (pH 7.5), 120 mM NaCl, 1 mM EDTA, 1% Triton X-100, and 1% NP-40] was supplemented with 3 μM olaparib to prevent the artificial activation of PARP (*63*). Poly/mono–ADP-ribosylated proteins were detected by Western blotting with an anti-rabbit poly/mono-ADP ribose antibody (Cell Signaling Technology).

NAD⁺ assay
Breast cancer cells were plated in a 96-well plate and exposed to vehicle or the PARP inhibitor olaparib (3 μM) for 30 min followed by L-arginine (50 mM) for 1 hour. To specifically assess NAD^+ levels, cells in PBS were lysed with 1% dodecyltrimethylammonium bromide in 0.2 N NaOH. Next, 0.4 HCl was added to the cells followed by incubation at 60°C for 15 min. Plates were then equilibrated at room temperature for 10 min, and 0.5 M tris base was added to neutralize the acid. Afterward, NAD^+ levels were assessed by using the NAD/NADH-Glo assay (Promega) according to the manufacturer's instructions. Luminescence was measured using a Synergy4 microplate reader (BioTek).

Colony formation assay
Specified numbers of cells were seeded in six-well plates (in triplicates) and let to recover for 12 hours followed by L-arginine (50 mM) or vehicle for 1 hour followed by a dose range of gamma radiation (from 1 to 6 Gy). After irradiation, cells were placed back in the tissue culture incubator and allowed to form colonies for 10 to 20 days. After verification of visible colony formation, wells were simultaneously fixed and stained with a 0.1% crystal violet:20% ethanol solution at room temperature, rinsed with water, and let to dry overnight. Crystal violet–stained colonies with at least 50 cells were counted. After correcting for plating efficiency, the survival fraction was calculated and fitted to a linear-quadratic model. For experiments with a single dose of ionizing radiation, cells were treated with vehicle, the NOS2 inhibitor 1400W (50 μM for 1.5 hours), and L-arginine (50 mM for 1 hour), alone or in combination, before exposure to ionizing radiation (2 Gy).

DNA damage levels
Alkaline comet assay was used to assess oxidized bases in the presence of Fpg and DNA single-strand breaks, double-strand breaks, and alkali-labile sites, as previously described (*64*). DNA damage was assessed 1 hour after exposure to L-arginine (50 mM) but before irradiation and at 30 min and 4 hours following ionizing radiation (4 Gy). For experiments with etoposide, DNA damage was measured after 2 hours of continuous exposure and after 1.5 and 6 hours of drug washout. Two slides per condition were analyzed in each experiment, and about 100 comets per slide were scored. Statistical analyses were carried out using the Kruskal-Wallis test followed by post hoc tests for multiple comparisons.

DNA damage foci analysis

Cells were seeded on coverslips in 12-well plates, treated with 50 mM L-arginine for 1 hour, and irradiated with a single dose of 2 Gy. After fixation and blocking in 10% normal blocking serum at room temperature, slides were incubated with rabbit anti–phosphorylated histone H2AX antibody (Cell Signaling Technology) at 4°C overnight or rabbit anti-TP53BPI (Cell Signaling Technology) and then incubated with secondary anti-rabbit fluorochrome-conjugated antibody. Nuclei were stained with TO-PRO-3 at room temperature. DNA double-strand breaks were evidenced by γH2AX foci formation. The average number of foci per cell was determined 30 min after irradiation.

DNA synthesis

Cells were seeded into 12-well plates in culture medium (25,000 cells per well) and treated with L-arginine (50 mM for 1 hour) and/or the competitive NOS inhibitor L-NMMA (200 μM for 1 hour). Quantification of cellular DNA synthesis was performed by 5-bromo-2′-deoxyuridine (Sigma Chemical) incorporation assessed with an LSRII flow cytometer coupled with FACSDiva software (BD Biosciences).

Flow cytometry and γH2AX level assessment

Murine tumors were harvested, and single-cell suspension was obtained by digesting tissues with ACK lysis buffer followed by filtering with a 30-μm cell strainer. Cells were then stained following a standard protocol. Briefly, cells were blocked with Fc block and incubated with primary antibody against CD45 (BioLegend). Cells were then permeabilized for staining with antibody against γH2AX (BioLegend) and against cleaved caspase-3 (BD Biosciences). Labeled cell populations were analyzed with an LSRII flow cytometer coupled with FACSDiva software (BD Biosciences). Unstained and single-color stained samples were used to determine appropriate gates, voltages, and compensations required.

Statistics

For the clinical trial, the primary end point was NPFS and the secondary end points were response rate, safety, PFS, OS, and tumor lactate peak. Response rate was considered as a result of complete responses plus partial responses over number of patients. Survival curves were obtained by the Kaplan-Meier method and compared by two-sided Cox-Mantel test. All analyses were conducted in an intention-to-treat basis. Parameters are presented as mean with the 95% confidence interval, unless specifically stated. For the preclinical experiments, unless specifically stated, data represent the mean with SEM of three independent experiments with replicates. P values are associated with a t test with two-tailed distribution of equal variance or nonparametric equivalent test when appropriate or one-way ANOVA followed by Bonferroni posttest for multiple comparisons based on experimental design. The P values cited were two-sided, and $P < 0.05$ was judged as statistically significant. Calculations were done with the statistics software Statistix (Analytical Software) or Prism v9.0 (GraphPad) or statistical packages for R.

SUPPLEMENTARY MATERIALS

Supplementary material for this article is available at https://science.org/doi/10.1126/sciadv.abg1964

View/request a protocol for this paper from *Bio-protocol*.

REFERENCES AND NOTES

1. X. Lin, L. M. DeAngelis, Treatment of brain metastases. *J. Clin. Oncol.* **33**, 3475–3484 (2015).
2. F. G. Kamar, J. B. Posner, Brain metastases. *Semin. Neurol.* **30**, 217–235 (2010).
3. B.-H. Nam, S. Y. Kim, H.-S. Han, Y. Kwon, K. S. Lee, T. H. Kim, J. Ro, Breast cancer subtypes and survival in patients with brain metastases. *Breast Cancer Res.* **10**, R20 (2008).
4. H. Illum, D. H. Wang, J. E. Dowell, W. J. Hittson, J. R. Torrisi, J. Meyer, S. Huerta, Phase I dose escalation trial of nitroglycerin in addition to 5-fluorouracil and radiation therapy for neoadjuvant treatment of operable rectal cancer. *Surgery* **158**, 460–465 (2015).
5. X. Gao, D. Saha, P. Kapur, T. Anthony, E. H. Livingston, S. Huerta, Radiosensitization of HT-29 cells and xenografts by the nitric oxide donor DETANONOate. *J. Surg. Oncol.* **100**, 149–158 (2009).
6. S. Huerta, G. Baay-Guzman, C. R. Gonzalez-Bonilla, E. H. Livingston, S. Huerta-Yepez, B. Bonavida, In vitro and in vivo sensitization of SW620 metastatic colon cancer cells to CDDP-induced apoptosis by the nitric oxide donor DETANONOate: Involvement of AIF. *Nitric Oxide Biol. Chem.* **20**, 182–194 (2009).
7. O. Arrieta, M. Blake, M. D. de la Mata-Moya, F. Corona, J. Turcott, D. Orta, J. Alexander-Alatorre, D. Gallardo-Rincón, Phase II study. Concurrent chemotherapy and radiotherapy with nitroglycerin in locally advanced non-small cell lung cancer. *Radiother. Oncol. J. Eur. Soc. Ther. Radiol. Oncol.* **111**, 311–315 (2014).
8. S. Ning, M. Bednarski, B. Oronsky, J. Scicinski, S. J. Knox, Novel nitric oxide generating compound glycidyl nitrate enhances the therapeutic efficacy of chemotherapy and radiotherapy. *Biochem. Biophys. Res. Commun.* **447**, 537–542 (2014).
9. J. B. Mitchell, D. A. Wink, W. DeGraff, J. Gamson, L. K. Keefer, M. C. Krishna, Hypoxic mammalian cell radiosensitization by nitric oxide. *Cancer Res.* **53**, 5845–5848 (1993).
10. M. Y. Janssens, D. L. Van den Berge, V. N. Verovski, C. Monsaert, G. A. Storme, Activation of inducible nitric oxide synthase results in nitric oxide-mediated radiosensitization of hypoxic EMT-6 tumor cells. *Cancer Res.* **58**, 5646–5648 (1998).
11. R. J. Griffin, C. M. Makepeace, W. J. Hur, C. W. Song, Radiosensitization of hypoxic tumor cells in vitro by nitric oxide. *Int. J. Radiat. Oncol. Biol. Phys.* **36**, 377–383 (1996).
12. B. F. Jordan, V. Grégoire, R. J. Demeure, P. Sonveaux, O. Feron, J. O'Hara, V. P. Vanhulle, N. Delzenne, B. Gallez, Insulin increases the sensitivity of tumors to irradiation: Involvement of an increase in tumor oxygenation mediated by a nitric oxide-dependent decrease of the tumor cells oxygen consumption. *Cancer Res.* **62**, 3555–3561 (2002).
13. B. F. Jordan, J. Peeterbroeck, O. Karroum, C. Diepart, J. Magat, V. Grégoire, B. Gallez, Captopril and S-nitrosocaptopril as potent radiosensitizers: Comparative study and underlying mechanisms. *Cancer Lett.* **293**, 213–219 (2010).
14. B. F. Jordan, P. Sonveaux, O. Feron, V. Grégoire, N. Beghein, C. Dessy, B. Gallez, Nitric oxide as a radiosensitizer: Evidence for an intrinsic role in addition to its effect on oxygen delivery and consumption. *Int. J. Cancer* **109**, 768–773 (2004).
15. J. O. Lundberg, E. Weitzberg, M. T. Gladwin, The nitrate-nitrite-nitric oxide pathway in physiology and therapeutics. *Nat. Rev. Drug Discov.* **7**, 156–167 (2008).
16. O. Thews, D. K. Kelleher, P. Vaupel, No improvement in perfusion and oxygenation of experimental tumors upon application of vasodilator drugs. *Int. J. Oncol.* **19**, 1243–1247 (2001).
17. F. U. Nielsen, S. Topp, M. R. Horsman, J. Overgaard, H. Stødkilde-Jørgensen, R. J. Maxwell, Localized in vivo 1H NMR spectroscopy of murine tumours: Effect of blood flow reduction. *NMR Biomed.* **12**, 175–183 (1999).
18. S. A. Glynn, B. J. Boersma, T. H. Dorsey, M. Yi, H. G. Yfantis, L. A. Ridnour, D. N. Martin, C. H. Switzer, R. S. Hudson, D. A. Wink, D. H. Lee, R. M. Stephens, S. Ambs, Increased NOS2 predicts poor survival in estrogen receptor-negative breast cancer patients. *J. Clin. Invest.* **120**, 3843–3854 (2010).
19. J. L. Heinecke, L. A. Ridnour, R. Y. S. Cheng, C. H. Switzer, M. M. Lizardo, C. Khanna, S. A. Glynn, S. P. Hussain, H. A. Young, S. Ambs, D. A. Wink, Tumor microenvironment-based feed-forward regulation of NOS2 in breast cancer progression. *Proc. Natl. Acad. Sci. U.S.A.* **111**, 6323–6328 (2014).
20. D. Fukumura, S. Kashiwagi, R. K. Jain, The role of nitric oxide in tumour progression. *Nat. Rev. Cancer* **6**, 521–534 (2006).
21. C.-F. Chang, A. R. Diers, N. Hogg, Cancer cell metabolism and the modulating effects of nitric oxide. *Free Radic. Biol. Med.* **79**, 324–336 (2015).
22. X. Le, D. Wei, S. Huang, J. R. J. Lancaster, K. Xie, Nitric oxide synthase II suppresses the growth and metastasis of human cancer regardless of its up-regulation of protumor factors. *Proc. Natl. Acad. Sci. U.S.A.* **102**, 8758–8763 (2005).
23. P. Clarkson, M. R. Adams, A. J. Powe, A. E. Donald, R. McCredie, J. Robinson, S. N. McCarthy, A. Keech, D. S. Celermajer, J. E. Deanfield, Oral L-arginine improves endothelium-dependent dilation in hypercholesterolemic young adults. *J. Clin. Invest.* **97**, 1989–1994 (1996).
24. H. Drexler, A. M. Zeiher, K. Meinzer, H. Just, Correction of endothelial dysfunction in coronary microcirculation of hypercholesterolaemic patients by L-arginine. *Lancet* **338**, 1546–1550 (1991).
25. M. A. Creager, S. J. Gallagher, X. J. Girerd, S. M. Coleman, V. J. Dzau, J. P. Cooke, L-arginine improves endothelium-dependent vasodilation in hypercholesterolemic humans. *J. Clin. Invest.* **90**, 1248–1253 (1992).

26. Y. Koga, Y. Akita, J. Nishioka, S. Yatsuga, N. Povalko, Y. Tanabe, S. Fujimoto, T. Matsuishi, L-arginine improves the symptoms of strokelike episodes in MELAS. *Neurology* **64**, 710–712 (2005).

27. R. D. Ganetzky, M. J. Falk, 8-year retrospective analysis of intravenous arginine therapy for acute metabolic strokes in pediatric mitochondrial disease. *Mol. Genet. Metab.* **123**, 301–308 (2018).

28. M. K. Koenig, L. Emrick, A. Karaa, M. Korson, F. Scaglia, S. Parikh, A. Goldstein, Recommendations for the management of strokelike episodes in patients with mitochondrial encephalomyopathy, lactic acidosis, and strokelike episodes. *JAMA Neurol.* **73**, 591–594 (2016).

29. H. Fujimoto, Y. Ando, T. Yamashita, H. Terazaki, Y. Tanaka, J. Sasaki, M. Matsumoto, M. Suga, M. Ando, Nitric oxide synthase activity in human lung cancer. *Jpn. J. Cancer Res.* **88**, 1190–1198 (1997).

30. S. Loibl, G. von Minckwitz, S. Weber, H.-P. Sinn, V. B. Schini-Kerth, I. Lobysheva, F. Nepveu, G. Wolf, K. Strebhardt, M. Kaufmann, Expression of endothelial and inducible nitric oxide synthase in benign and malignant lesions of the breast and measurement of nitric oxide using electron paramagnetic resonance spectroscopy. *Cancer* **95**, 1191–1198 (2002).

31. H. C. Ludwig, R. Ahkavan-Shigari, S. Rausch, K. Schallock, C. Quentin, D. Ziegler, V. Bockermann, E. Markakis, Oedema extension in cerebral metastasis and correlation with the expression of nitric oxide synthase isozymes (NOS I-III). *Anticancer Res.* **20**, 305–310 (2000).

32. D. Basudhar, G. Bharadwaj, V. Somasundaram, R. Y. S. Cheng, L. A. Ridnour, M. Fujita, S. J. Lockett, S. K. Anderson, D. W. McVicar, D. A. Wink, Understanding the tumour micro-environment communication network from an NOS2/COX2 perspective. *Br. J. Pharmacol.* **176**, 155–176 (2019).

33. P. D. Bos, X. H.-F. Zhang, C. Nadal, W. Shu, R. R. Gomis, D. X. Nguyen, A. J. Minn, M. J. van de Vijver, W. L. Gerald, J. A. Foekens, J. Massagué, Genes that mediate breast cancer metastasis to the brain. *Nature* **459**, 1005–1009 (2009).

34. S. M. Bode-Böger, R. H. Böger, A. Galland, D. Tsikas, J. C. Frölich, L-arginine-induced vasodilation in healthy humans: Pharmacokinetic-pharmacodynamic relationship. *Br. J. Clin. Pharmacol.* **46**, 489–497 (1998).

35. L. Castillo, T. E. Chapman, Y. M. Yu, A. Ajami, J. F. Burke, V. R. Young, Dietary arginine uptake by the splanchnic region in adult humans. *Am. J. Phys.* **265**, E532–E539 (1993).

36. L. Castillo, L. Beaumier, A. M. Ajami, V. R. Young, Whole body nitric oxide synthesis in healthy men determined from [15N] arginine-to-[15N]citrulline labeling. *Proc. Natl. Acad. Sci. U.S.A.* **93**, 11460–11465 (1996).

37. S. C. Forbes, G. J. Bell, The acute effects of a low and high dose of oral L-arginine supplementation in young active males at rest. *Appl. Physiol. Nutr. Metab.* **36**, 405–411 (2011).

38. F. Galli, S. Rovidati, L. Ghibelli, F. Canestrari, S-nitrosylation of glyceraldehyde-3-phosphate dehydrogenase decreases the enzyme affinity to the erythrocyte membrane. *Nitric Oxide Biol. Chem.* **2**, 17–27 (1998).

39. J. M. Souza, R. Radi, Glyceraldehyde-3-phosphate dehydrogenase inactivation by peroxynitrite. *Arch. Biochem. Biophys.* **360**, 187–194 (1998).

40. M. R. White, E. D. Garcin, D-glyceraldehyde-3-phosphate dehydrogenase structure and function. *Subcell. Biochem.* **83**, 413–453 (2017).

41. E. P. Garvey, J. A. Oplinger, E. S. Furfine, R. J. Kiff, F. Laszlo, B. J. Whittle, R. G. Knowles, 1400W is a slow, tight binding, and highly selective inhibitor of inducible nitric-oxide synthase in vitro and in vivo. *J. Biol. Chem.* **272**, 4959–4963 (1997).

42. P. Pacher, J. S. Beckman, L. Liaudet, Nitric oxide and peroxynitrite in health and disease. *Physiol. Rev.* **87**, 315–424 (2007).

43. P. Pacher, C. Szabo, Role of the peroxynitrite-poly(ADP-ribose) polymerase pathway in human disease. *Am. J. Pathol.* **173**, 2–13 (2008).

44. J. J. Arroyo-Crespo, A. Armiñán, D. Charbonnier, C. Deladriere, M. Palomino-Schätzlein, R. Lamas-Domingo, J. Forteza, A. Pineda-Lucena, M. J. Vicent, Characterization of triple-negative breast cancer preclinical models provides functional evidence of metastatic progression. *Int. J. Cancer* **145**, 2267–2281 (2019).

45. M. Wu, A. Neilson, A. L. Swift, R. Moran, J. Tamagnine, D. Parslow, S. Armistead, K. Lemire, J. Orrell, J. Teich, S. Chomicz, D. A. Ferrick, Multiparameter metabolic analysis reveals a close link between attenuated mitochondrial bioenergetic function and enhanced glycolysis dependency in human tumor cells. *Am. J. Physiol. Cell Physiol.* **292**, C125–C136 (2007).

46. W. Ying, NAD+/NADH and NADP+/NADPH in cellular functions and cell death: Regulation and biological consequences. *Antioxid. Redox Signal.* **10**, 179–206 (2008).

47. A. A. Pieper, A. Verma, J. Zhang, S. H. Snyder, Poly (ADP-ribose) polymerase, nitric oxide and cell death. *Trends Pharmacol. Sci.* **20**, 171–181 (1999).

48. C.-H. Tang, W. Wei, L. Liu, Regulation of DNA repair by S-nitrosylation. *Biochim. Biophys. Acta* **1820**, 730–735 (2012).

49. J. A. Nickoloff, N. Sharma, L. Taylor, Clustered DNA double-strand breaks: Biological effects and relevance to cancer radiotherapy. *Genes (Basel)* **11**, 99 (2020).

50. Y. S. Cho-Chung, T. Clair, J. S. Bodwin, B. Berghoffer, Growth arrest and morphological change of human breast cancer cells by dibutyryl cyclic AMP and L-arginine. *Science* **214**, 77–79 (1981).

51. C. N. Hinrichs, M. Ingargiola, T. Käubler, S. Löck, A. Temme, A. Köhn-Luque, A. Deutsch, O. Vovk, O. Stasyk, L. A. Kunz-Schughart, Arginine deprivation therapy: Putative strategy to eradicate glioblastoma cells by radiosensitization. *Mol. Cancer Ther.* **17**, 393–406 (2018).

52. B. Vynnytska-Myronovska, Y. Bobak, Y. Garbe, C. Dittfeld, O. Stasyk, L. A. Kunz-Schughart, Single amino acid arginine starvation efficiently sensitizes cancer cells to canavanine treatment and irradiation. *Int. J. Cancer* **130**, 2164–2175 (2012).

53. P. K. Singh, A. A. Deorukhkar, B. P. Venkatesulu, X. Li, R. Tailor, J. S. Bomalaski, S. Krishnan, Exploiting arginine auxotrophy with pegylated arginine deiminase (ADI-PEG20) to sensitize pancreatic cancer to radiotherapy via metabolic dysregulation. *Mol. Cancer Ther.* **18**, 2381–2393 (2019).

54. R. K. Jain, Determinants of tumor blood flow: A review. *Cancer Res.* **48**, 2641–2658 (1988).

55. P. Sonveaux, C. Dessy, A. Brouet, B. F. Jordan, V. Grégoire, B. Gallez, J.-L. Balligand, O. Feron, Modulation of the tumor vasculature functionality by ionizing radiation accounts for tumor radiosensitization and promotes gene delivery. *FASEB J.* **16**, 1979–1981 (2002).

56. Y. S. Cho-Chung, T. Clair, J. S. Bodwin, D. M. Hill, Arrest of mammary tumor growth in vivo by L-arginine: Stimulation of NAD-dependent activation of adenylate cyclase. *Biochem. Biophys. Res. Commun.* **95**, 1306–1313 (1980).

57. R. Geiger, J. C. Rieckmann, T. Wolf, C. Basso, Y. Feng, T. Fuhrer, M. Kogadeeva, P. Picotti, F. Meissner, M. Mann, N. Zamboni, F. Sallusto, A. Lanzavecchia, L-arginine modulates T cell metabolism and enhances survival and anti-tumor activity. *Cell* **167**, 829–842.e13 (2016).

58. J. Shukla, S. Chatterjee, V. S. Thakur, S. Premachandran, R. Checker, T. B. Poduval, L-Arginine reverses radiation-induced immune dysfunction: The need for optimum treatment window. *Radiat. Res.* **171**, 180–187 (2009).

59. C. Harmon, C. O'Farrelly, M. W. Robinson, The immune consequences of lactate in the tumor microenvironment. *Adv. Exp. Med. Biol.* **1259**, 113–124 (2020).

60. Y. Dong, R. Eskandari, C. Ray, K. L. Granlund, L. Dos Santos-Cunha, V. Z. Miloushev, S. S. Tee, J. Jeong, O. Aras, Y.-B. Chen, E. H. Cheng, J. J. Hsieh, K. R. Keshari, Hyperpolarized MRI visualizes warburg effects and predicts treatment response to mTOR inhibitors in patient-derived ccRCC xenograft models. *Cancer Res.* **79**, 242–250 (2019).

61. F. Dieterle, A. Ross, G. Schlotterbeck, H. Senn, Probabilistic quotient normalization as robust method to account for dilution of complex biological mixtures. application in 1H NMR metabonomics. *Anal. Chem.* **78**, 4281–4290 (2006).

62. Y. Benjamini, Y. Hochberg, Controlling the false discovery rate: A practical and powerful approach to multiple testing. *J. R. Stat. Soc. Ser. B* **57**, 289–300 (1995).

63. Y. Zhang, J. Wang, M. Ding, Y. Yu, Site-specific characterization of the Asp- and Glu-ADP-ribosylated proteome. *Nat. Methods* **10**, 981–984 (2013).

64. R. Marullo, E. Werner, H. Zhang, G. Z. Chen, D. M. Shin, P. W. Doetsch, HPV16 E6 and E7 proteins induce a chronic oxidative stress response via NOX2 that causes genomic instability and increased susceptibility to DNA damage in head and neck cancer cells. *Carcinogenesis* **36**, 1397–1406 (2015).